HHS Public Access

Author manuscript

Metab Eng. Author manuscript; available in PMC 2022 January 16.

Published in final edited form as:

Metab Eng. 2022 January ; 69: 231–248. doi:10.1016/j.ymben.2021.12.003.

Metabolic flux analysis of the non-transitory starch tradeoff for lipid production in mature tobacco leaves☆

Kevin L. Chu[a,1], **Somnath Koley**[a,1], **Lauren M. Jenkins**[a], **Sally R. Bailey**[a,b], **Shrikaar Kambhampati**[a], **Kevin Foley**[a], **Jennifer J. Arp**[a], **Stewart A. Morley**[a,b], **Kirk J. Czymmek**[a], **Philip D. Bates**[c], **Doug K. Allen**[a,b,*]

[a] Donald Danforth Plant Science Center, St. Louis, Missouri, 63132, USA

[b] United States Department of Agriculture–Agriculture Research Service, Donald Danforth Plant Science Center, St. Louis, Missouri, 63132, USA

[c] Institute of Biological Chemistry, Washington State University, Pullman, WA, 99164-6340, USA

Abstract

The metabolic plasticity of tobacco leaves has been demonstrated via the generation of transgenic plants that can accumulate over 30% dry weight as triacylglycerols. In investigating the changes in carbon partitioning in these high lipid-producing (HLP) leaves, foliar lipids accumulated stepwise over development. Interestingly, non-transient starch was observed to accumulate with plant age in WT but not HLP leaves, with a drop in foliar starch concurrent with an increase in lipid content. The metabolic carbon tradeoff between starch and lipid was studied using $^{13}CO_2$-labeling experiments and isotopically nonstationary metabolic flux analysis, not previously applied to the mature leaves of a crop. Fatty acid synthesis was investigated through assessment of acyl-acyl carrier proteins using a recently derived quantification method that was extended to accommodate isotopic labeling. Analysis of labeling patterns and flux modeling indicated the continued production of unlabeled starch, sucrose cycling, and a significant contribution of NADP-malic enzyme to plastidic pyruvate production for the production of lipids in HLP leaves, with the latter verified by enzyme activity assays. The results suggest an inherent capacity for a developmentally regulated carbon sink in tobacco leaves and may in part explain the uniquely successful leaf lipid engineering efforts in this crop.

☆The author responsible for distribution of materials integral to the findings presented in this article in accordance with the policy described in the Guide for Authors is: Doug K. Allen (doug.allen@ars.usda.gov)

* Corresponding author. United States Department of Agriculture–Agriculture Research Service, Donald Danforth Plant Science Center, St. Louis, Missouri, 63132, USA. doug.allen@ars.usda.gov (D.K. Allen).

[1]These authors contributed equally to this work.

Author contributions

D.K.A. and P.D.B. conceived the original research plans; K.L.C., L.M. J., and S.R.B. performed the experiments, with assistance from S.Ka, K. F., and J.A.; S.Ko and K.L.C. performed flux modeling, with assistance from D.K.A.; K.L.C., S.Ko, L.M.J., S.Ka, K.F., and D.K.A. analyzed the data and contributed to scope; L.M.J. contributed expertise for the acyl-ACP approach; S.A.M. and K.L.C. conducted NADP-malic enzyme assays; K.J.C. performed all microscopy analysis; and K.L.C. and D.K.A. wrote the article with contribution from P.D.B. and was approved by all authors.

Declaration of competing interest

None.

Appendix A. Supplementary data

Supplementary data to this article can be found online at https://doi.org/10.1016/j.ymben.2021.12.003.

Keywords

Carbon partitioning; Starch-triacylglycerol tradeoff; *Nicotiana tabacum* (tobacco); Acyl-ACPs; Metabolic flux analysis; ^{13}C isotope Labeling

1. Introduction

Photosynthetic leaves are the primary organ for carbon assimilation, producing metabolites for local needs or exporting sugars and amino acids to other tissues. Leaves convert atmospheric carbon dioxide (CO_2) to reduced organic metabolic intermediates and storage reserves through the Calvin-Benson cycle (CBC) (Bassham et al., 1954), the source of precursors for biomass components including polysaccharides, lipids, amino acids for protein, and nucleotides for DNA and RNA (McClain and Sharkey, 2019; Raines and Paul, 2006; Smith and Stitt, 2007; Stitt and Zeeman, 2012). A mature photosynthetic leaf primarily produces two major carbon outputs in different spatial locations: starch in the chloroplast via the ADP-glucose glucosyl-donor and sucrose in the cytosol from UDP-glucose and fructose 6-phosphate (Stitt and Quick, 1989).

Starch is synthesized in leaves during the day to act as a temporary carbon storage reserve that is remobilized at night for cellular respiration or conversion to sucrose to sustain nocturnal growth in sink tissues (Geiger and Servaites, 1994; Zeeman et al., 2010; Stitt and Zeeman, 2012; Ludewig and Flügge, 2013; Smith and Zeeman, 2020). In *Arabidopsis thaliana,* 30–50% of assimilated carbon is converted to starch (Zeeman et al., 2010), depending on photoperiod length (Mengin et al., 2017). The regulation of starch levels is important to maximize carbon use efficiency and avoid starvation during the night. Starch levels follow a diurnal pattern in Arabidopsis leaves, such that changing day and night lengths results in altered linear rates of starch production and turnover, with about 95% of the starch being consumed by the end of the night (Lu et al., 2005; Smith and Stitt, 2007; Gibon et al., 2009; Graf et al., 2010; Graf and Smith, 2011; Mengin et al., 2017). This tight control over starch turnover may be relaxed during long-day photoperiods (Baerenfaller et al., 2015; Sulpice et al., 2014), with starch turnover occurring alongside synthesis in the light to prevent overaccumulation and maintain optimal levels of sucrose for the start of the light-dark transition (Fernandez et al., 2017).

Diel patterns of foliar starch accumulation and degradation similar to Arabidopsis are understood to be the standard model of starch regulation due to their wide occurrence in many crop species including *Beta vulgaris*, *Phaseolus vulgaris* (Fondy and Geiger, 1982), Spinacia oleracea (Stitt et al., 1983), *Zea mays* (Kalt-Torres and Huber, 1987), and *Solanum tuberosum* (Lorenzen and Ewing, 1992). Less common have been reports that starch accumulates with plant age and persists at the end of the night in the leaves of a few plant species such as *Nicotiana tabacum* and *Lotus japonicus* (Häusler et al., 1998; Matheson and Wheatley, 1963; Vriet et al., 2010). Starch persistence at daybreak, however, does not inherently suggest non-transient starch accumulation as it may simply be a consequence of delayed starch turnover under long photoperiods (Matt et al., 1998), nutrient stresses (Morcuende et al., 2007; Rufty et al., 1988), or sink-limited conditions

(Grimmer et al., 1999; Hädrich et al., 2012; Pilkington et al., 2015; Scialdone et al., 2013). Non-transient starch reserves have also been demonstrated in leaf growth zones as a buffer against perturbations (Czedik-Eysenberg et al., 2016) as well as in older plants during reproductive growth (Lauxmann et al., 2016). Potentially significant variation of diel starch patterns within the same plant species depending on plant age, growth conditions (including photoperiod), and genotype (Ruckle et al., 2017) can further confound studies regarding starch trends. There is little coverage or acknowledgement of non-transient starch accumulation in major starch reviews and textbooks, suggesting an important gap in our common understanding of plant growth processes which complicates studies on photosynthetic carbon partitioning in plants.

Relative to starch, triacylglycerols (TAG) are a more energetically valuable carbon storage reserve in plants, reaching over 80% dry weight (DW) in oil palm mesocarp and 20–50% DW in seeds of common oilseed crops (Baud and Lepiniec, 2010; Bourgis et al., 2011; Weselake et al., 2009). Most leaves, however, accumulate only 2–5% of their DW biomass as lipids, primarily in the form of galactolipids for chloroplast membranes. Less than 1.5% of the total lipid in leaves is in the form of energy-dense TAGs (Allen et al., 2015; Koiwai et al., 1983; Li-Beisson et al., 2013; Yang and Ohlrogge, 2009), where they play important roles in membrane lipid homeostasis and temporarily store free fatty acids released during senescence and various abiotic stresses (Arisz et al., 2018; Fan et al., 2014, 2017; Ischebeck et al., 2020; Kaup et al., 2002). Studies of lipid accumulation in oilseeds and vegetative tissues have identified a number of key targets for manipulation either directly involved in or influencing TAG biosynthesis including the transcription factor WRI1 that regulates glycolytic carbon flow into fatty acid biosynthetic pathways (Baud et al., 2009; Cernac and Benning, 2004), the transcription factor LEC2 that acts as a master regulator of oilseed maturation and embryogenesis (Santos Mendoza et al., 2005; Stone et al., 2001), the acyl-CoA:diacylglycerol acyltransferase DGAT1 responsible for the final step in TAG biosynthesis (Jako et al., 2001; Routaboul et al., 1999; Zou et al., 1999), and OLEOSIN proteins that coat and stabilize oil bodies in oilseeds (Huang, 1996; Scott et al., 2010).

Efforts to engineer increased production and accumulation of TAG in both oilseeds and vegetative tissues for more energy-dense biomass have achieved the most success through the combined targeting of multiple aspects of developmental central carbon metabolism to fatty acid synthesis (‘Push’), the incorporation of those fatty acids into TAG biosynthesis (‘Pull’), and stabilization of lipid droplets and minimization of TAG turnover (‘Package and Protect’) (Beechey-Gradwell et al., 2019; Durrett et al., 2008; Parajuli et al., 2020; Slocombe et al., 2009; Vanhercke et al., 2014b, 2019b; Weselake, 2016; Xu and Shanklin, 2016), with synergistic increases in TAG yields in vegetative tissues often observed when multiple genes are simultaneously targeted (Kelly et al., 2013; Vanhercke et al., 2013; Winichayakul et al., 2013; Zale et al., 2016). The highest elevated TAG yields in leaves reported thus far (reviewed in Vanhercke et al., 2019b) have been achieved in engineered tobacco lines (Andrianov et al., 2010; Cai et al., 2019; Vanhercke et al., 2014a, 2017; Zhou et al., 2020), with some high lipid-producing (HLP) lines producing over 30% foliar TAG (DW) without drastic consequences on plant growth. Metabolic explanations for carbon partitioning in these lines, however, are incomplete, are not quantitative or mechanistic,

and do not indicate why engineering efforts are more successful in certain plant species compared to others.

Stable isotope tracer labeling studies using ^{13}C in combination with metabolic flux analysis (MFA) enable quantitative mapping of *in vivo* intracellular carbon fluxes in a metabolic network. Steady-state MFA is a standard method for investigating metabolism (Allen and Young, 2013; Lonien and Schwender, 2009; Masakapalli et al., 2013; Ratcliffe and Shachar-Hill, 2006; Schwender et al., 2015) but is not applicable to autotrophic tissues as photosynthetic metabolites are uniformly labeled at steady-state and uninformative (Shastri and Morgan, 2007). In addition, day/night cycles constrain pseudo steady-state metabolism to limited periods within the photoperiod. Carbon uptake in plant leaf tissues is further restricted to CO_2 due to the carbon source nature of mature photosynthetic leaves. Isotopically nonstationary metabolic flux analysis (INST-MFA) using transient $^{13}CO_2$ labeling studies is thus necessary for studying leaf carbon fluxes. INST-MFA has previously been performed primarily to map autotrophic metabolism in photosynthetic cyanobacteria (Abernathy et al., 2017, 2019; Hendry et al., 2017; Young et al., 2011). Although $^{13}CO_2$-labeling has been performed in tobacco leaves to study photosynthetic metabolic turnover (Hasunuma et al., 2010) and steady-state MFA has been conducted in tobacco roots (Masakapalli et al., 2014), the application of INST-MFA to leaves is limited to prior investigations in Arabidopsis leaves (Ma et al., 2014) and very recently to camelina (Xu et al., 2021).

The current study describes non-transient starch accumulation in addition to diel fluctuations in tobacco leaves with plant age. The metabolic tradeoff of these starch reserves with lipid production for the production of next generation biofuel crops was investigated through quantitative carbon partitioning studies and flux maps comparing *Nicotiana tabacum* with the best-performing HLP transgenic tobacco line overexpressing *WR1*, *DGAT1*, *OLEOSIN*, and *LEC2* (Vanhercke et al., 2017). Lipid, starch, and soluble sugar levels were characterized in WT and HLP leaves over the photoperiod at different ages in vegetative development. The findings indicate that starch patterns in leaves from older tobacco plants deviate from the Arabidopsis paradigm of finely regulated diel synthesis/degradation. The capacity of tobacco leaves as a sink tissue that normally stores starch to shift to storing lipid provides an explanation for the high TAG levels achieved in this crop. Dynamic fluxes through central carbon metabolism as well as lipid synthesis were measured using $^{13}CO_2$-labeling experiments over long durations (*i.e.*, 5 h) to gauge the production and turnover of starch, sucrose, and fatty acid products in WT and HLP leaves. Fatty acid biosynthesis was assessed by tracking ^{13}C-labeling in acyl-ACP intermediates using a recently developed method for quantifying acyl-ACPs (Jenkins et al., 2021; Nam et al., 2020) modified to monitor ^{13}C-label incorporation. INST-MFA was applied to mature leaves of the crop plant tobacco. The labeling and flux analyses indicated continued production of unlabeled starch from active unlabeled ADP-glucose, sucrose cycling via vacuolar invertase, and a significant contribution from NADP-malic enzyme (NADP-ME) to plastidic pyruvate production in the HLP leaves that sustains the enhanced fatty acid biosynthesis needed for lipid production. Our results reveal major changes in central carbon metabolism that occur during the vegetative stage in oil-accumulating leaves and suggest why foliar lipid engineering efforts have been more successful in tobacco compared to other plant species.

2. Materials and methods

2.1. Plant growth and leaf collection

WT (Wisconsin 38) and transgenic HLP *Nicotiana tabacum* plants (described previously as *LEC2* (Vanhercke et al., 2017)) were germinated in a greenhouse at 27 °C/25 °C (day/night) with 60–90% humidity before being transplanted into 0.43 L pots containing Berger BM7 35% Bark HP soil mix (pH 5.5–6.5) at 3 weeks after sowing. Plants were grown during the winter months under 12 h/12 h light/dark conditions, with supplemental lighting activating whenever light readings dropped below 500 μmol*$m^{-2}s^{-1}$ in greenhouses at the Donald Danforth Plant Science Center, St. Louis, MO. 200 ppm Jacks 15–16-17 N–P–K Peat-Lite fertilizer was applied three times weekly. Multiple sets of leaf punches (8.5 mm in diameter) were collected from the apexes of the top expanded leaf (at or near full size) of four plants of each genotype at 26, 41, 55, 62, and 72 days after sowing (DAS). Sample collection was at noon unless otherwise indicated. The top expanded leaf for WT plants was leaf 8 at 41 DAS, leaf 11 at 55 DAS, leaf 13 at 63 DAS, and leaf 15 at 72 DAS. The top flat leaf, though not yet fully expanded, was leaf 6 for WT plants at 26 DAS. The top expanded leaf for HLP plants was always one leaf below that of WT due to delayed initial growth. The collected leaf discs were frozen in liquid nitrogen and stored at −80 °C until further processing. For starch and lipid assays, leaf discs were further lyophilized for 2 days at −50 °C on a Labconco FreeZone freeze dryer before extraction. The tips of the top expanded leaves were sampled to avoid shading and minimize any import of photosynthate from other areas as tobacco leaves mature photosynthetically from tip to base, a process that leads to loss of phloem import capacity (Turgeon, 2006). To rule out any effects of small pot size on starch accumulation due to sink-limitation and other stresses, WT plants were also transplanted into 1.1 and 1.9 L pots. Starch measurements at dawn in mature plants were found to be similar regardless of pot size.

2.2. Lipid measurements

Total lipid levels were measured from 10 to 15 mg of lyophilized leaf tissue using a protocol modified from Allen and Young (2013) (see Supplemental Methods). Comparisons of peak areas to C15:0 and C17:0 TAG internal standards were used for quantification. Carbon compositions of 77.2% and 76.8% were determined for WT and HLP lipids respectively, utilizing their measured fatty acid distributions and formulas when calculating biomass as carbon (Supplemental Datasheet 4).

2.3. Starch assay

The total concentration of foliar starch from 10 to 15 mg lyophilized powdered leaf tissue was determined with the Megazyme starch assay kit (Megazyme International Ireland), using the AOAC Official Method 996.11 (McCleary et al., 1997, 2019) modified to adjust the final assay volume for a 96-well plate (Supplemental Methods). Sample concentrations were determined using a maize starch standard curve processed alongside leaf samples. A carbon composition of 42.9% was used for starch when calculating biomass as carbon, utilizing the chemical formula for maltotriose.

2.4. Metabolite extraction and quantification

Soluble sugars, sugar phosphates, organic acids, and free amino acids were extracted with methanol/chloroform/water using a protocol modified from Ma et al. (2017) (Supplemental Methods), taking care to keep samples chilled throughout. The extracted filtered samples were run on an AB Sciex QTRAP 6500 mass spectrometer linked to a Shimadzu HPLC, with ions being detected and monitored using a targeted multiple-reaction monitoring (MRM) approach. Metabolites were eluted and run using parameters as previously described (Czajka et al., 2020), using positive ionization for amino acids and negative ionization for all other metabolites. Protein quantification was performed by directly hydrolyzing the protein from leaf samples and quantifying the resulting individual amino acids as previously described (Kambhampati et al., 2019). Metabolite concentrations and recoveries were calculated based on external calibration curves and internal standards (PIPES for sugar phosphates and organic acids, ribitol for sugars, and norvaline for amino acids). A $1/x^2$ weighting factor was applied for external calibration curves as suggested by Gu et al. (2014).

2.5. $^{13}CO_2$ labeling

$^{13}CO_2$ labeling studies were performed on greenhouse-grown plants at 62–65 DAS. The tips of the top expanded leaves of WT and HLP plants (leaves 13 and 12, respectively) were clamped in custom-made transparent cylindrical labeling chambers (vol. = 50.7 cm^3) for labeling using premixed gas containing $^{13}CO_2$ at a$^{13}CO_2/N_2/O_2$ ratio of 0.033:78:21.967 (Aldrich) with a flow rate of 0.5 L/min. The leaf was positioned in the labeling chamber such that roughly even amounts of tissue were present on either side of the midvein with a small gap left on the side of the leaf closest to the exit hole opposite the gas inlet. The portion of the leaf within the chamber was marked during labeling. After providing leaves with label for either 5, 15, or 300 min, the leaf was removed from the labeling chamber and rapidly quenched (~0.5 s) using a metal freeze-clamp prechilled in liquid nitrogen. The frozen leaf sections were then dropped onto a prechilled metal plate where the labeled leaf section was isolated before being coarsely ground and stored at −80 °C. The same procedures were carried out in parallel on the top expanded leaves of unlabeled control plants. All labeling experiments were carried out from late morning to mid-afternoon (10 a.m.−4 PM), with a WT and a HLP leaf being labeled simultaneously for a total of three plants of each genotype labeled on successive days. After extracting metabolites, their isotopologue distributions were determined via LC-MS/MS (Ma et al., 2017), with correction for natural ^{13}C abundance performed as previously described (Fernandez et al., 1996).

Labeled starch isotopologues were calculated by multiplying isotopologue abundance with the average pool sizes of starch-digested glucose measured with the Megazyme kit. ^{13}C starch content was determined by summing the amounts of labeled isotopologues as previously described (Arrivault et al., 2016; Fernandez et al., 2017), except the analysis of labeled isotopologues was directly performed on digested starch glucose. The amount of ^{13}C in metabolites was determined by multiplying the calculated amount of each labeled isotopologue by the number of labeled carbons in each isotopologue and summing the results as previously described (Arrivault et al., 2016).

2.6. Acyl-ACP extraction

Acyl-ACPs were precipitated using a protocol as previously described (Jenkins et al., 2021; Nam et al., 2020; see Supplemental Methods for parameters). 30 or 60 mg of ground fresh leaf tissue for WT and HLP, respectively, were utilized for extraction. The digested acyl-ACP molecules were identified using MRM parameters as previously described, with the addition of ^{13}C-labeled isotopologues for the acyl chains.

2.7. Model network and flux determination

Metabolic models describing central carbon metabolism in photosynthetic leaves were constructed based on a previously published Arabidopsis rosette model (Ma et al., 2014), augmented by relevant reaction networks from the literature (see Supplemental Methods). Lists of abbreviations, constraints, and reactions used in the network model are provided in Supplemental Datasheets 1, 10, and 12. The MATLAB-based Isotopomer Network Compartmental Analysis (INCA) package (Version 1.9, Young, 2014) was used to estimate metabolic fluxes in the network models. Additional details on INCA parameters and runs are as previously described (Ma et al., 2014). Dilution parameters were incorporated to account for labeling dilutions due to the presence of metabolite pools inaccessible to ^{13}C over the course of the labeling experiments (Young et al., 2011; see Supplemental Datasheet 11). Since the flux maps are of mostly fully expanded photosynthetically competent leaves, changes in other biomass components such as protein, nucleic acids, and structural carbohydrates were likely negligible over the modeled time course, as in prior flux maps (Ma et al., 2014).

2.8. Microscopy analyses

Tissue samples were taken from the top expanded leaves of 67 DAS WT and HLP plants. For lipid droplet analyses, leaf samples were stained for 45 min in aqueous BODIPY 505/515 (1 μg/ml), fixed in 4% paraformaldehyde in PBS, rinsed three times in water, and mounted in 6% agar. 100 μm thick leaf cross-sections were generated (Vibratome 1500 Sectioning System) for imaging using a Leica SP8-X confocal microscope with a 63× HC Plan Apochromat water immersion objective (1.2 NA) and the pinhole set to 1 airy unit. The following excitation and emission wavelengths were used: 405 nm excitation and 415–450 nm emission for cell wall autofluorescence (cyan), 488 nm excitation and 500–550 nm emission for BODIPY-labeled lipid droplets (green), and 649 nm excitation and 659–779 nm emission for chlorophyll autofluorescence (magenta). Optical slices were collected at 1 μm z-intervals to create 3D maximum intensity projections. For confocal starch imaging, leaves were fixed in 4% paraformaldehyde in PBS, rinsed three times in water, extracted in 95% overnight at 50 °C, rehydrated and mounted in 6% agar. The agar block with leaf tissue was planned with a vibratome and the exposed leaf cross sections were stained in iodine (2% KI & 1% I_2 w/v) for 15 min, rinsed in water and imaged with a 63× HC Plan Apochromat water immersion objective (1.2 NA) and the pinhole set to 1 airy unit. Tissue was imaged with 488 nm excitation and 415–450 nm emission for cell wall autofluorescence (cyan), 488 nm excitation and 579–507 nm emission for starch (green), and 536–648 nm emission for autofluorescence (red). Optical slices were collected at 1 μm z-intervals to create 3D maximum intensity projections.

For sample preparation for electron microscopy, tobacco leaves were fixed, stained and embedded using a modified protocol for enhanced *en bloc* staining of large tissues (Hua et al., 2015). Briefly, 3 mm biopsy punches of leaves were fixed overnight with 2% glutaraldehyde and 2% paraformaldehyde with 0.1% Tween in 0.1 M sodium cacodylate buffer, pH 7.4, rinsed in 3X in buffer and fixed for 2 h in 1% OsO_4 in cacodylate buffer at room temperature. Samples were then transferred to 2.5% ferrocyanide in cacodylate buffer for 1.5 h, rinsed and placed in 1% thiocarbohydrazide (TCH, #21900; Electron Microscopy Sciences) in ddH_2O for 45 min at 40 °C. Samples were then fixed with 2% OsO_4 in ddH_2O for 1.5 h, rinsed 2X in ddH_2O and placed overnight in aqueous 1% uranyl acetate at 4 °C. The samples were then transferred to an oven at 50 °C for 2 h, rinsed, placed in lead aspartate at 50 °C for 2 h, rinsed, dehydrated in a graded series of acetone and embedded in Embed 812 hard formulation epoxy resin.

For serial block-face scanning electron microscopy (SBFEM), samples were mounted on a Gatan 3View aluminum pin with 2-part conductive silver epoxy (Circuit Works, CW2400), trimmed to minimize excess resin and imaged on a Zeiss GeminiSEM300 equipped with a Gatan 3View at 1.2 kV with focal charge compensation (Deerinck et al., 2018) using 8000 × 8000 pixel image size and 5 nm pixel size (x-y) and 50 nm slice thickness (z). For TEM, resin blocks were trimmed and directly mounted in the vise-chuck of a Leica Ultracut UCT ultramicrotome (Leica, Buffalo Grove, IL, USA). Ultrathin sections (~60 to 70 nm) were cut using a diamond knife (type ultra 35 °C; Diatome), mounted on copper grids (FCFT300-CU-50, VWR, Radnor, PA, USA). Samples were imaged with a LEO 912 AB Energy Filter Transmission Electron Microscope (Zeiss, Oberkochen, Germany). Micrographs were acquired with iTEM software (ver. 5.2) (Olympus Soft Imaging Solutions GmbH, Germany) with a TRS 2048 × 2048k slow-scan charge-coupled device (CCD) camera (TRÖNDLE Restlichtverstärkersysteme, Germany). Alternatively, EM resin sections were cut 300 nm thick, mounted on coverslips, stained (Epoxy Tissue Stain, #14590; Electron Microscopy Sciences) and imaged on a Nikon Ni-E upright microscope with a 20X Plan Apochromat (N.A. 0.75) air and 63X Plan Apochromat (N.A. 1.4) oil immersion objective lenses with a DS Fi3 CMOS color digital camera at 2880 × 2028 pixel frames size.

3. Results

3.1. Lipid levels increase over development in a stepwise manner

For developmental analysis of lipid production and accumulation, the top expanded leaves of WT and HLP tobacco plants grown in the greenhouse under a 12-h photoperiod were sampled at midday at 26, 41, 55, 62, and 72 days after sowing (DAS). HLP plants showed delayed seedling establishment and a 1/6th reduction in leaf size compared with WT plants but reached comparable heights by 55 DAS and flowered at similar times, with neither line flowering nor bolting until after 77 DAS. Older HLP leaves displayed leaf curling and developed a faint mottled yellow appearance that intensified with plant age, likely due to reduced chlorophyll levels (Fig. 1A). Enhanced lipid accumulation in HLP leaves (predominantly palmitic, oleic, and linoleic fatty acids (Fig. S1A)) occurred throughout development (Fig. 1B) but exhibited a dramatic increase late in development between 55 and 62 DAS, which were comparable to values reported previously at senescence (Vanhercke

et al., 2017). No major differences in lipid levels and composition were detected between dawn and dusk for either WT or HLP leaves at 62 DAS, indicating insignificant diurnal lipid turnover in either line (Fig. S1A). Confocal microscopy of 67 DAS leaves stained with BODIPY 505/515 showed large lipid droplets accumulating in HLP mesophyll cells (especially the palisade layer) that were not present in WT (Fig. 1C), illustrating differential lipid metabolism across leaf cell types. Plastoglobuli clustering was often observed in the chloroplasts of palisade mesophyll cells of HLP leaves but was more uncommon in WT chloroplasts (Fig. S1B), reflecting the increased demand for lipid synthesis and/or related stresses experienced by the HLP leaves.

Acyl-ACPs are hallmark intermediates in the synthesis and elongation of fatty acids, but levels of acyl-ACPs have not been previously quantified in tobacco leaves nor considered over the diurnal period. At 63 DAS, ACPs containing acyl chain lengths from 2 to 16 carbons were examined in both WT and HLP leaves over the photoperiod. The levels of most acyl-ACPs were higher in HLP than in WT and resulted in a greater amount of a terminal C16:0-ACP product (Fig. 1D). Though WT leaves showed no diurnal fluctuation, fatty acid synthesis was modestly elevated in the light in HLP leaves based on increased levels of acyl-ACPs.

3.2. WT leaves accumulate non-transient starch over development that disappears in HLP leaves

The top expanded leaves were also sampled for starch across the photoperiod at different plant ages during vegetative growth to analyze diel starch patterns across development. Foliar starch levels accumulated with plant age on top of diurnal fluctuations (Fig. 2). The amount of starch remaining at the end of night increased from 1.6% of DW at 41 DAS to 28.1% by 62 DAS before dropping to 19.2% at 72 DAS. This foliar starch pool at dawn is non-transient since most transient starch turnover is understood to occur during the night. Diurnal variations in starch, prominent in younger plants, became less pronounced with plant age due to starch accumulation. Leaf starch levels started rising again after the onset of dawn at all ages, indicating that starch values at the end of night timepoint are likely at or near their lowest point, unlike cases in tobacco plants grown under long-day photoperiods where starch continued to decline for the first few hours in the light and only started accumulating during the second half of the light period (Matt et al., 1998). Leaf starch levels in the HLP plants were initially slightly lower than WT but displayed similar diurnal patterns in younger plants. By 62 DAS, however, there was a significant drop in foliar starch at all timepoints to levels at or below those measured at 41 DAS (Fig. 2). Diurnal starch patterns, while still apparent, also showed a noticeable decrease in amplitude.

To investigate nocturnal starch turnover, nighttime levels of the disaccharide maltose were measured. The presence of maltose is characteristic of starch breakdown due to its unique position as an intermediate of starch degradation not commonly found elsewhere in metabolism (Niittylä et al., 2004; Weise et al., 2004). WT and HLP leaves were sampled at midnight every other day from 56 to 64 DAS, the period spanning the largest changes in starch and lipid levels. No significant differences among HLP maltose levels were detected across this period (Fig. 3A), indicating that increased rates of nighttime starch degradation

are unlikely to be the reason for the decrease in starch levels. Midnight levels of maltose were found to be higher in WT leaves compared to HLP, indicating either overall higher rates of starch turnover or decreased turnover of maltose itself due to lower metabolic demands in WT leaves. These observations are consistent with the generally lower diurnal starch patterns measured in HLP leaves.

3.3. Non-transient starch accumulation depletes with lipid production

The drop in foliar starch levels was roughly concurrent with the significant accumulation of lipids in HLP leaves at 62 DAS (Figs. 1B and 2), suggesting a change in foliar carbon sink production. Both sucrose (Fig. 3B) and protein (Fig. 3C) levels were largely consistent across development, indicating that HLP leaves accumulated lipids primarily at the expense of starch though there was also a minor contribution from free glucose and fructose (Fig. 3B and Fig. S2). The change in biomass carbon from altered TAG and starch levels was calculated utilizing a ~77% carbon composition for TAG based on the chemical formulas and proportions of the measured fatty acids (Supplemental Datasheet 4) and a 43% carbon composition for starch using the formula for maltotriose. 76% of the carbon from increased lipids was accounted for by the difference in starch per gram (DW) biomass at 62 DAS (Fig. 3D). Thus, the availability of a large pre-existing non-transient carbon reserve in foliar plastids of older tobacco plants offers an explanation as to how high oil-accumulating leaves can produce large amounts of lipids without drastic penalties to plant growth and viability.

3.4. A distinct ^{13}C-inaccessible pool of ADP-glucose is responsible for significant starch production

Since both biomass accumulation and acyl-ACP measurements indicated a large increase in HLP foliar lipid production concurrent with a decrease in foliar starch at the 9-week age, plants at this stage were utilized for subsequent $^{13}CO_2$-labeling studies and metabolic flux analysis. Transient labeling of leaves with a$^{13}CO_2$ gas mixture was performed to quantify real-time starch biosynthesis and assess photosynthetic carbon fluxes through central carbon metabolic pathways. Total starch accumulation during 5 h labeling experiments was compared with ^{13}C-labeled starch accumulation similar to a prior investigation (Fernandez et al., 2017). WT leaves synthesized greater amounts of starch, including ^{13}C-labeled starch, than HLP over the labeling period (Fig. 4), consistent with reallocation of carbon resources for lipid production in oil accumulating leaves. In the case of the HLP plants, the percent ^{13}C-enrichment of starch glucosyl units was actually higher than in WT leaves (Fig. 4B); however, this was a consequence of smaller preexisting starch levels to dilute relative labeling (Fig. 4A and C).

Labeled starch production was lower than total starch production in both WT and HLP leaves (Fig. 4D). This large proportion of unlabeled starch production indicates that significant starch turnover simultaneous with synthesis in the light as previously described in Arabidopsis (Fernandez et al., 2017) cannot explain the lower starch levels in HLP tobacco leaves. If significant daytime starch turnover occurred, the amount of ^{13}C-starch produced over the labeling period should exceed the measured total starch production. Thus, the decrease in foliar starch levels with lipid production does not appear to be due to elevated

rates of either daytime or nighttime starch turnover and is instead a result of altered starch synthesis.

The starch glucosyl-donor ADP-glucose is a plastidic intermediate with a small pool size that labels rapidly (Figs. S3 and S4). ADP-glucose reached ~70% ^{13}C-enrichment after only 15 min of $^{13}CO_2$-labeling in both WT and HLP leaves (Fig. S3) but then did not label much further over the course of 5 h. The lack of further ^{13}C labeling increase in ADP-glucose between 15 min and 5 h of labeling in WT leaves (Fig. 5 and Fig. S3) combined with the relatively high proportion of the unlabeled isotopologue of ADP-glucose remaining in WT after 5 h of labeling (Fig. 6) and the large amount of unlabeled starch produced over 5 h (Fig. 4D), indicates the continued production of unlabeled starch, possibly as a second pool inaccessible to $^{13}CO_2$ over the labeling period. Analysis of the isotopologue distributions of ADP-glucose and digested starch glucose after 5 h of labeling further suggest contribution from active unlabeled (i.e., ^{13}C-inaccessible) ADP-glucose pools in addition to ^{13}C-labeled pools for starch production, rather than any unintended incorporation of unlabeled $^{12}CO_2$ during the quenching/sampling process as this would not immediately affect the unlabeled (M0) isotopologue of ADP-glucose. Separating the unlabeled isotopologue of ADP-glucose from the labeled (ΣM1-M6) isotopologues and comparing the recalculated distributions with the 5 h starch isotopologue patterns (Supplemental Datasheet 6) indicated that most of the ADP-glucose pool was labeled by $^{13}CO_2$ (88% in WT and 97% in HLP); however, the remaining unlabeled (M0) pool was also metabolically active and produced the majority of the starch synthesized over the 5 h labeling experiment regardless of whether the leaves were producing high amounts of lipid (Fig. 6). The small proportion of the total ADP-glucose pool that was unlabeled thus had a higher metabolic turnover rate than the labeled ADP-glucose to support unlabeled starch production. In HLP leaves, the M0 isotopologue of ADP-glucose present after 5 h of labeling was lower than WT (Fig. 6) and resulted in a reduced active unlabeled ADP-glucose pool, consistent with the reduced production of unlabeled starch (Fig. 4D).

The data indicated the presence of separate active pools of ADP-glucose, with spatially separated unlabeled metabolite intermediates in cell types that do not directly utilize atmospheric CO_2. Conceptually, two further lines of evidence support this conclusion. First, RuBP that is specific to the CBC contained very little unlabeled M0 after 5 h of labeling whereas other intermediates (e.g., sedoheptulose-7-phosphate, triose phosphates and hexose phosphates) which are not exclusive to CBC metabolism continued to contain an unlabeled M0 component at the end of labeling (Supplemental Datasheet 8), supporting the concept of unlabeled starch biosynthesis in separate cell types from unlabeled intermediates via the pentose phosphate pathway that are disconnected from the CBC entry point of RuBP. Second, microscopy analyses indicated increased abundance and size of starch granules in the bundle-sheath and vascular parenchyma cells of WT leaves compared to HLP (Fig. 7) that can utilize unlabeled carbon transported in the vasculature as previously observed (Hibberd and Quick, 2002).

3.5. Differences in HLP metabolite labeling patterns suggest different carbon flux patterns

Though the reduced starch production was consistent with the postulated tradeoff of carbon for lipid biosynthesis, the labeling data for central metabolites was not always consistent with expectations of photosynthetic carbon flow. Prior to metabolic flux analysis, the rates of labeled carbon through central carbon metabolites were estimated by calculating the amount of ^{13}C in the metabolites (Fig. 5) as previously described (Arrivault et al., 2016), in addition to considering average ^{13}C-enrichment (Fig. S3) and metabolite pool size data (Fig. S4) (Ma et al., 2014; Szecowka et al., 2013). Calculation of n atom ^{13}C equivalents g^{-1} FW enabled labeling comparisons between central metabolites in plants accumulating lipid or starch while limiting some potentially confounding differences in metabolite pool sizes and contribution of inactive pools. Isotopic labeling resulted in some of the expected differences through metabolic pathways. For example, labeled carbon in the CBC/pentose phosphate pathway intermediates sedoheptulose-7-phosphate and dihydroxyacetone phosphate was lower in HLP leaves relative to WT (Fig. 5 and Fig. S3), consistent with the reduced net carbon assimilation in HLP (Supplemental Datasheet 10) and decreased total vegetative biomass observed in the greenhouse (Vanhercke et al., 2017). However, labeled carbon in hexose phosphates including ADP-glucose, the sucrose precursor UDP-glucose, and glucose 6-phosphate was elevated in HLP leaves despite decreased starch production and similar sucrose pool sizes (Figs. 3B, 4 and 5). The total amount of sucrose, UDP-glucose, and ADP-glucose did not change over the course of the labeling experiment for either WT or HLP (Figs. S2C and S4, Supplemental Datasheet 9), suggesting similar partitioning towards sucrose and starch occurred over the labeling period. The discrepancy in carbon partitioning between photosynthetic CBC metabolites and downstream carbohydrate intermediates as well as the unlabeled starch fraction was specifically studied through metabolic flux analysis. The studies were designed to more specifically assess the source of unlabeled starch and other precursor metabolites with inactive or unlabeled pools by utilizing a long 5 h labeling timepoint.

The $^{13}CO_2$ transient labeling experiment provided a unique opportunity to inspect the fatty acid biosynthesis process through the detection and quantification of isotope incorporation into acyl-ACPs. Dynamic movement of labeled carbons through the acyl portions of acyl-ACPs were higher in HLP leaves (Fig. 5), indicating increased flux through fatty acid synthesis that is consistent with FAME data at 62 DAS. The increased proportion of labeled acyl isotopologues in HLP is consistent with the hypothesis that more ^{13}C from the CBC cycle was directed towards fatty acid synthesis in these leaves. Labeling in WT acyl-ACPs leveled off at an average ^{13}C-enrichment of 20% by 5 h (Fig. S3), indicating a significant portion of carbon flux to acyl-ACPs does not come directly from the CBC in WT plants (possibly involving relatively unlabeled organic acid intermediates from the vacuole) or that a pool of acyl-ACPs is ^{13}C-inaccessible and may not participate in ‘active’ metabolism (Allen and Young, 2020). Deciphering the input of both labeled and unlabeled carbon sources contributed to the construction of network maps for flux modeling.

3.6. Model construction for metabolic flux analysis in photosynthetic tobacco leaves

To quantify the differences in carbon partitioning, computational metabolic flux maps were generated based on ^{13}C-labeling using INST-MFA. Models were constructed from measured isotopologue distributions of central carbon metabolites (and included labeled acyl-ACPs and starch glucose) at different labeling timepoints, net CO_2 assimilation, and labeled starch production rates. Boundaries for labeled starch production from labeled ADP-glucose were calculated using ADP-glucose and starch isotopologues (Supplemental Datasheet 10), and export fluxes of sucrose and amino acids were based on ratios obtained from previous *Nicotiana* phloem sap measurements (Brugière et al., 1999; Hocking, 1980). The reaction network was similar to that reported for an illuminated Arabidopsis leaf (Ma et al., 2014) which included the CBC, photorespiratory bypass, TCA cycle, and biosynthetic routes for starch, sucrose, and phloem amino acids; but also incorporated additional pathways for acyl-ACP biosynthesis. Other minor differences from the Arabidopsis model are described in Supplemental Methods.

3.7. Metabolic responses to high oil production confirm rerouting of carbohydrate carbon to lipids

The flux maps indicated decreased carbon fluxes to starch and sucrose and increased fluxes to acetyl-CoA and fatty acid production in HLP leaves independent of lipid pool size data and without needing to impose any constraints on lipid fluxes, thus providing validation of the network and flux values (Fig. 8). The rate of carbon flux into starch and sucrose synthesis as a proportion of net assimilation in WT leaves (89%) was also similar to values from previous labeling studies (Sharkey et al., 1985). As expected, the model indicated essentially no carbon flux to fatty acid production in a mature photosynthetic WT leaf. The increased demand for acetyl-CoA units to make fatty acids in HLP leaves was somewhat provided by enhanced flux from phosphoenolpyruvate (PEP) to plastidic pyruvate, with increased import of cytosolic PEP into the chloroplasts. More significantly, plastidic NADP-malic enzyme (ME) made the majority of the contribution (75%) to plastidic pyruvate production in HLP leaves, with plastidic NADP-malic enzyme activity being necessary to explain both the high M2 isotopologue of C4-ACP and the discrepancy in labeling between pyruvate and the more labeled downstream alanine that is produced from cytosolic pyruvate (Fig. 9). When unlabeled malate is used to produce some of the pyruvate, the conversion of pyruvate to acetyl-CoA results in both unlabeled and M2 labeled acetyl-CoA that, when combined, enhance the M2 isotopologue in the C4-ACP profile more than otherwise expected. The modeled plastidic fraction of pyruvate was elevated in the HLP leaves (55–91% in HLP vs 0–6% in WT, Supplemental Datasheet 15), with a greater percentage of M0 isotopologue that was derived from the less labeled malate pool imported into the plastid (Facchinelli and Weber, 2011). Carbon flux through cytosolic PEP carboxylase to oxaloacetate (OAA) and subsequent conversion to malate via malate dehydrogenase was also elevated in HLP leaves to compensate for the increased utilization of malate for plastidic pyruvate synthesis, with the elevated labeling in HLP aspartate (Supplemental Datasheet 8) offering further support since aspartate and malate share the same OAA precursor. Higher malic enzyme flux was validated by increased enzymatic activity observed in HLP leaf extracts as measured by both spectrophotometric assays and label incorporation

into pyruvate from supplied ^{13}C-malate (Fig. S5). The increased ME flux in HLP was only associated with the plastid location (Fig. 8).

Total amino acid export fluxes to the phloem were similar between WT and HLP leaves. Fluxes through RuBisCO carboxylation and the Calvin-Benson cycle were lower in HLP leaves (Fig. 8A), as expected from the lower net CO_2 assimilation rates measured by a LI-6800 photosynthesis system (Supplemental Datasheet 10) and labeling patterns of Calvin-Benson cycle metabolites (Fig. 5). Photorespiration, characterized by Vo/Vc, decreased from 0.26 in WT leaves, values within range of previous reports in tobacco (Bellasio et al., 2014; Bernacchi et al., 2001; Walker et al., 2013; Whitney et al., 2011), to 0.18 in HLP leaves, likely reflecting the increased concentrations of CO_2 released in the plastid leading to increased RuBisCO carboxylation relative to oxygenation (Fig. 8B). The HLP flux map had elevated plastidic CO_2 production that comprised almost half of the total metabolic CO_2 production. The flux maps also showed that the decreased contribution of unlabeled vacuolar hexose to the hexose phosphate pool during sucrose cycling explained the increased labeling observed in G6P and UDP-glucose (Fig. 5) in HLP, a conclusion corroborated by the decreased hexose pool sizes in HLP leaves (Fig. 3B). The data thus provides *in planta* evidence of sucrose cycling via vacuolar invertase that confirms previous *in vitro* activity assays from tobacco leaf extracts that found vacuolar invertase to be the major source of sucrose cycling in tobacco leaves at midday (Huber, 1989; Moore et al., 1998), as the majority of free hexose is vacuolar (Moore et al., 1997). Model results were further validated through confirmation of the ADP-glucose dilution from the flux maps (Supplemental Datasheet 15) that closely matched the proportions of active unlabeled ADP-glucose independently calculated from isotopologue distributions for both WT and HLP (Fig. 6).

4. Discussion

Our classical understanding of foliar starch metabolism based on numerous studies in Arabidopsis is that rates of starch synthesis and turnover are tightly regulated to ensure that most of the starch produced during the day is consumed by the end of the night. The current study describes the accumulation of a basal pool of non-transient foliar starch throughout tobacco vegetative growth. To explore the possible metabolic plasticity of this starch, we characterized WT tobacco leaves and compared them with leaves from a high lipid-producing transgenic tobacco line, considering that the developmental starch accumulation in WT leaves may be an important contributor to the successful high foliar oil phenotype in the transgenic plants. Metabolic flux analysis was applied to investigate why tobacco is so amenable to foliar lipid engineering, as TAG yields in transgenic tobacco leaves have far surpassed levels achieved in other plant species even when similar transgene combinations were manipulated. The combination of studies resulted in a number of metabolic insights including: 1) the presence of an active unlabeled ADP-glucose pool responsible for producing a significant proportion of starch, 2) vacuolar sucrose cycling, and 3) the significant contribution of malic enzyme to plastidic pyruvate production in HLP leaves to sustain the increased fatty acid synthetic rates. INST-MFA was applied to mature tobacco leaves, utilizing a long labeling timepoint (5 h) and incorporating acyl-ACP

information specific to fatty acid biosynthesis to examine dramatic tradeoffs in lipid and starch partitioning as well as explaining metabolite pools that remained unlabeled.

4.1. Isotopically labeled acyl-ACPs provide a means to assess the dynamics of fatty acid biosynthesis in high oil leaves and indicated elevated daytime production of lipids

An often overlooked aspect in the assessment of metabolism is that accumulation over time reflects both biosynthesis and metabolic turnover events (Allen, 2016a; 2016b). Frequently the accumulated level of a storage reserve such as lipid can be measured easily, but such measures do not capture the amount that may be turned over and can underestimate biosynthesis if turnover is not negligible. Acyl-ACPs are specific components to the fatty acid biosynthetic process and represent a conclusive measure of fatty acid production when combined with isotopic labeling. Our results provide evidence of elevated fluxes through fatty acid synthesis in HLP leaves that validate the observed increase in lipid accumulation at the 9-week age (Figs. 1 and 5). The elevated daytime pools of HLP acyl-ACPs (Fig. 1D) indicated that most of the increased lipid production occurs during the day, consistent with the increased activity in the light of the acetyl-CoA carboxylase enzyme responsible for the first committed step in fatty acid synthesis (Browse et al., 1981; Sasaki et al., 1997; Sauer and Heise, 1984; Ye et al., 2020).

4.2. Metabolic underpinnings of starch-lipid tradeoff can be resolved with INST-MFA

The flux maps indicated a 92% carbon tradeoff from starch to lipid production in photosynthetic cells of HLP leaves (Supplemental Datasheet 13). In revealing the alterations in photosynthetic carbon fluxes in HLP leaves, INST-MFA was able to resolve differences in the labeling patterns of HLP metabolites. Labeling in the carbohydrate intermediates G6P, UDP-glucose, and ADP-glucose was similar between the lines (Fig. 5, Figs. S3 and S4) even though starch production in HLP was reduced and decreased labeling was observed in CBC intermediates. The flux modeling, along with analysis of isotopologue distributions (Figs. 6 and 8), indicated a smaller diluting (unlabeled) ADP-glucose pool in HLP leaves as well as a decreased contribution of unlabeled vacuolar hexose to the cytosolic hexose phosphate pool during sucrose cycling explain the differences. Sucrose cycling was clear from the high proportion of half-labeled sucrose isotopologues (Fig. S6) and was analogous to half-labeled acyl-ACP products that were also observed. Although sucrose cycling may appear to be an energetically wasteful futile cycle, sucrose cycling has been demonstrated to play roles in sugar sensing and regulation of photosynthesis (Goldschmidt and Huber, 1992; Weiszmann et al., 2018). Levels of sucrose, fructose, and glucose do not vary significantly over the photoperiod (Fig. S2), suggesting that sucrose cycling occurs primarily via acid invertase within the vacuole, with some of the resulting hexoses being exported out of the vacuole for subsequent (re)synthesis of sucrose. Further evidence for invertase-mediated sucrose cycling is provided by the lower label incorporation in glucose at the end of the labeling period compared to hexose phosphate, UDP-glucose, and sucrose (Fig. S6). The potential contribution the G6P shunt (Sharkey et al., 2020; Sharkey and Weise, 2016) may play in contributing to labeling patterns is discussed in Supplemental Text, Part I.

The long labeling timepoints in the current study also provided more conclusive analyses of organic acid and TCA metabolism. Metabolites such as malate label slowly due to the

combination of large organic acid pool sizes and low fluxes relative to CBC (Tcherkez et al., 2009); thus the flow through TCA metabolism is difficult to resolve with shorter time course experiments. Consistent with other measurements of limited day respiration in illuminated photosynthetic leaves (Abadie et al., 2017; Ma et al., 2014; Tcherkez et al., 2009), TCA pathway activity was found to be essentially acyclic in both WT and HLP leaves (Fig. 8A), with no flux found between α-ketoglutarate and malate (Supplemental Datasheet 13).

Flux models did not predict any flux through plastidic enolase in WT leaves, consistent with previous reports of an incomplete glycolytic pathway in photosynthesizing leaves (Prabhakar et al., 2009; Stitt and Ap Rees, 1979) with plastidic PEP believed to be imported from the cytosol (Baud, 2018). However, expression analyses on leaves of the high oil tobacco parent line (overexpressing the same genes except *LEC2*) indicate upregulated plastidic enolase expression (Vanhercke et al., 2017), with the 35% upper bound of this flux in HLP (Supplemental Datasheet 13) leaving open the possibility that this line may have activated this step (normally reserved for non-photosynthetic tissues such as seeds) for the production of fatty acids due to the significant requirement for acetyl-CoA. NADP-malic enzyme was found to play a major role in providing plastidic pyruvate for fatty acid synthesis in the HLP leaves (Fig. 8A). While C4-ACP isotopologue patterns at 5 h indicated the involvement of two differentially labeled precursor pools to explain the high proportions of the M2 isotopologue, the labeling data suggests that the metabolite dilution involves the production of plastidic pyruvate via NADP-malic enzyme in addition to pyruvate kinase (Müller et al., 2008) instead of acetyl-CoA production via ATP citrate lyase (ACL) as the presence of a plastidic isoform of ACL in plants is unclear (Fatland et al., 2000, 2002; Rangasamy and Ratledge, 2000). The decreased labeling observed in HLP pyruvate compared to alanine offered further evidence for plastidic ME activity as alanine is produced from cytosolic pyruvate and thus should not exhibit higher labeling than its precursor without unlabeled pyruvate also being produced in another organelle (Fig. 9). The increased activity of the plastidic isoform of malic enzyme has previously been reported in high oil plant embryos and oilseeds during active lipid deposition (Allen et al., 2009; Allen and Young, 2013; Cocuron et al., 2019; Gerrard Wheeler et al., 2016; Kang and Rawsthorne, 1994; Smith et al., 1992; Tsogtbaatar et al., 2020) and was validated by independent measurements (Fig. S5), supporting the increased flux predicted by modeling and the larger malate pool size in HLP leaves (Supplemental Datasheet 9). The production of malate from OAA in the cytosol and subsequent conversion to pyruvate within the chloroplast would additionally shuttle reducing equivalents important for enhanced plastidic fatty acid biosynthesis. The results thus suggest increasing plastidic NADP-malic enzyme activity as a potential target for future efforts to engineer increased lipid in vegetative tissues.

It is intriguing to speculate that the increased release of CO_2 in the chloroplast stroma of HLP leaves from fatty acid synthesis may be recaptured by RuBisCO when mesophyll conductance is limiting photosynthesis, thus aiding RuBisCO carboxylation relative to oxygenation. This hypothesis is partially supported by the lower rates of photorespiration determined in HLP plants by MFA. Observations from A^*C_i curves (Supplemental Datasheet 16) conducted at our growth and experimental conditions demonstrate that net assimilation continues to increase with CO_2 concentrations past atmospheric levels for both WT and HLP greenhouse-grown plants, thus indicating that photosynthesis is in

the RuBisCO-limiting portion of the A*Ci curve and thus still responsive to increases in CO_2 concentration. In addition, the CO_2 compensation point of HLP leaves was increased compared to WT, indicative of the increased internal CO_2 release from fatty acid synthesis. This is briefly discussed in Supplemental Text, Part II. The potential requirement for photorespiration as a “safety valve” to dissipate excess reducing power via catalase (Stuhlfauth et al., 1990) would also be decreased in HLP chloroplasts due to increased NADPH usage for fatty acid synthesis that is only partially met by NADP-malic enzyme. In NAD-ME and NADP-ME subtype C4 plants, kinetic modeling indicates that decarboxylation via malic enzymes are driven by the NAD $(P)^+$/NAD(P)H ratios (Bräutigam et al., 2018). Here, demand by fatty acid synthesis for NADPH is offset by the combination of NADP-malic enzyme and pyruvate dehydrogenase that together provide the stoichiometric amount for each acetyl group used in fatty acid synthesis, with additional CBC demands most likely balanced by photosystem II-based production. The oxidized redox poise (Bräutigam et al., 2018) may thus help establish the relative contribution of malic enzyme flux that is balanced with lipid production, the CBC, and photorespiration.

4.3. Unexpected carbon fluxes through ADP-glucose and starch reflect spatiotemporal differences in metabolism

Analysis of ADP-glucose and starch isotopologues suggested that a small proportion of unlabeled ADP-glucose had a high metabolic turnover and was responsible for producing the majority of the unlabeled starch over the labeling period (Fig. 6 and Supplemental Datasheet 6), likely in distinct intercellular locations. This cellular heterogeneity was more apparent in WT tobacco leaves due to the increased proportion of ^{13}C-inaccessible ADP-glucose. The substantial amount of unlabeled starch produced during the labeling period was further validated by independent calculations of unlabeled starch production using peak area abundances of starch glucose isotopologues, with the resulting rates of total starch synthesis also comparable to rates derived from separate diurnal starch studies (Supplemental Datasheet 17). Import of unlabeled photosynthate from the base of the leaf or other source leaves is unlikely due to the largely irreversible basipetal cessation of photoassimilate import capacity during leaf maturation (Ding et al., 1988; Turgeon and Webb, 1976).

Distinct intercellular compartmentalization of starch production has been suggested by others. It is known that tobacco bundle-sheath cells can utilize carbon from the vasculature to produce starch (Hibberd and Quick, 2002) that could partially account for the unlabeled ADP-glucose fraction (Fig. S8), with bundle-sheath starch potentially accumulating to significant levels relative to mesophyll cells in C_3 plants (Miyake, 2016; Miyake and Maeda, 1976). Microscopy analyses (Fig. 7A and B, Fig. S9A) of leaf cross-sections show decreased starch distribution in HLP cells compared to WT, particularly in the bundle-sheath cells surrounding the vascular bundle. Starch granules were also present in WT phloem cells within the vasculature that were absent in corresponding HLP cells which were instead filled with lipid droplets (Fig. 7C). Both bundle-sheath and phloem cells thus provide potential cellular locations for unlabeled starch production. The large amounts of oil bodies in HLP phloem cells (visible in both cross- and longitudinal sections (Figs. S9B and S9C)) could also be synthesized using unlabeled carbon sources from within the vasculature or

could be produced within neighboring cells and subsequently exported into the phloem, as suggested by the presence of oil bodies in bundle-sheath cells immediately adjacent to these phloem cells (Fig. 7B). Assimilation of unlabeled CO_2 transported via the xylem could also make a minor contribution to unlabeled metabolites (Stutz and Hanson, 2019). Alternatively, the synthesis of secondary metabolites in glandular trichome cells, which can be quite significant in tobacco leaves (up to 30% DW; Wagner, 1991), releases CO_2 that could be fixed by trichome RuBisCO specialized to refix this released CO_2 rather than atmospheric CO_2 (Laterre et al., 2017). This unlabeled CO_2 could provide a portion of the unlabeled primary metabolites that contribute to the M0 isotopologues remaining after 5 h of labeling (Supplemental Dataset 8) or even lead to the production of unlabeled starch granules within the trichomes (Konarska and Łotocka, 2020), reflecting the increased cellular heterogeneity and secondary metabolite production in older leaves; however, such explanations for the current analysis are speculative. These alternate sources of unlabeled carbon may nonetheless be insufficient to explain the large proportion of carbon flux for unlabeled starch production relative to photosynthetic carbon fixation and thus warrant further investigation.

4.4. Older tobacco leaves display strong carbon metabolic plasticity

HLP leaves displayed a drop in foliar starch that coincides with enhanced lipid accumulation, suggesting a tradeoff in carbon that was confirmed by lower rates of starch production (Fig. 4D) and a shift in carbon flux from starch to fatty acid production (Fig. 8). Our finding that WT tobacco leaves accumulate large amounts of non-transient starch with plant age sheds new insight on the understanding of foliar starch regulation in a canopied crop as a divergence from the commonly accepted diurnal paradigm. While excess starch accumulation due to sink limitations (Arp, 1991) is a particularly relevant concern in the case of a crop like tobacco that has been bred for leafy biomass production rather than seed yield, starch accumulation persisting at dawn in mature leaves was observed across a range of different pot sizes and has even been reported for field-grown tobacco (Matheson and Wheatley, 1963), suggesting that this phenomenon is not solely attributable to limitations inherent in the growth conditions used in the current study. Indeed, we have also observed starch accumulation in non-mesophyll tissues of older tobacco plants at dawn and similar observations in Arabidopsis (Lauxmann et al., 2016) have generated hypotheses about reproductive growth. Thus, non-transient starch is a more prevalent feature than commonly acknowledged with as yet unexplored roles and regulation. This basal starch pool thus provides a ready pool of stored carbon in the chloroplasts for lipid synthesis that does not appear to be required for normal carbon source tissue functions, as diel starch fluctuations still occurred in HLP leaves (Fig. 2) and sucrose levels were largely unchanged (Fig. 3B and Fig. S2C; see Supplemental Text, Part III). The lack of an excess starch pool in young HLP plants which still produce large amounts of lipid may partially explain the hindered growth during establishment (Mitchell et al., 2020). Although redirection of carbon from starch to lipid has been previously demonstrated in Arabidopsis leaves via the combination of lipid engineering with mutants deficient in starch synthesis (Sanjaya et al., 2011; Yu et al., 2018; Zhai et al., 2017), the enhanced lipid levels did not come close to those achieved in transgenic tobacco leaves. Thus, the large non-transitory starch pools present in older tobacco leaves provide a plausible explanation as to why leaf lipid engineering efforts have

proven most successful in tobacco. Relatively little carbon could be expected to be shunted to lipid from the tightly regulated Arabidopsis leaf starch without drastically affecting plant growth and viability, likely explaining the more modest increases in TAG yields obtained in transgenic Arabidopsis plants with the same genes targeted (Kelly et al., 2013; Zhai et al., 2017). A recent study engineering similar gene combinations in grain sorghum leaves (Vanhercke et al., 2019a) has also fallen short of the high lipid yields achieved in tobacco, further emphasizing the importance of a pre-existing carbon pool in achieving high foliar TAG yields.

We have shown that tobacco leaves from older WT plants are metabolically acting as dual source-sink tissues, synthesizing sucrose for export while also producing and storing non-transient starch. Since younger HLP plants showed delayed growth and lower lipid accumulation when foliar starch was more transient, the amount of lipid that can be produced was limited by the energetic costs required for daily life. The developmental accumulation of non-transient starch in older tobacco plants allows for increased metabolic plasticity of carbon sources, with oil-producing leaves simply substituting one form of stored carbon (starch) for another (TAGs). Thus, future efforts to engineer lipid production in vegetative tissues will need to consider the current capacity of the crop to store starch or other carbon reserves in vegetative tissues and, based on the current study, may be particularly relevant in sink-limited plants or conditions. Sugarcane offers an encouraging case due to its accumulation of sucrose within internode stalks (Parajuli et al., 2020; Zale et al., 2016), though further efforts will be needed to match tobacco leaf lipid yields despite the potentially increased sink potential of stem tissue. The localization of the tobacco starch carbon pool in chloroplasts likely can provide a more direct switch to oil production than the sugarcane sucrose pool compartmentalized in vacuoles and the apoplast. Our findings indicate that a better understanding of plants that accumulate large non-essential “sink” pools of carbon-rich metabolites in their vegetative tissues could provide promising new platforms for vegetative oil crops.

Supplementary Material

Refer to Web version on PubMed Central for supplementary material.

Acknowledgements

We thank Dr. Xue-Rong Zhou (Commonwealth Scientific and Industrial Research Organisation (CSIRO)) for providing WT and HLP transgenic tobacco seeds; Dr. Howard Berg (Integrated Microscopy Facility/Advanced Bioimaging Laboratory, Donald Danforth Plant Science Center) for preliminary microscopy efforts, Dr. Brad Evans and Jon Mattingly (Proteomics and Mass Spectrometry Facility, Donald Danforth Plant Science Center) for their assistance with LC-MS instrumentation; and Kevin Reilly, Kris Haines, Matt Adams, and Aileen Wok (Integrated Plant Growth Facility, Donald Danforth Plant Science Center) for their assistance with plant growth and propagation. We also thank the reviewers for their thoughtful comments that improved the manuscript. We acknowledge imaging support from the Advanced Bioimaging Laboratory at the Danforth Plant Science Center. The Leica SPX-8 confocal microscope used was acquired through National Science Foundation Major Research Instrumentation grant (DBI-1337680) while the QTRAP LC-MS/MS used was acquired through (DBI-1427621). The authors acknowledge support for aspects of this work from United States Department of Agriculture-Agricultural Research Service, United States Department of Agriculture-National Institute of Food and Agriculture grant awards (2021–67013-33778, 2017–67013-26156, and 2016–67013-24585), National Science Foundation awards (MCB-1616820, IOS-1829365, and IOS-1812235), and National Institutes of Health award (U01 CA235508). No conflicts of interest are declared.

Abbreviations

ACP	acyl carrier protein
DAS	days after sowing
HLP	high lipid-producing
INST-MFA	isotopically nonstationary metabolic flux analysis
ME	malic enzyme
TAG	triacylglycerol
ZT	Zeitgeber time

References

Abadie C, Lothier J, Boex-Fontvieille E, Carroll A, Tcherkez G, 2017. Direct assessment of the metabolic origin of carbon atoms in glutamate from illuminated leaves using 13C-NMR. New Phytol. 216, 1079–1089. 10.1111/nph.14719. [PubMed: 28771732]

Abernathy MH, Czajka JJ, Allen DK, Hill NC, Cameron JC, Tang YJ, 2019. Cyanobacterial carboxysome mutant analysis reveals the influence of enzyme compartmentalization on cellular metabolism and metabolic network rigidity. Metab. Eng. 54, 222–231. 10.1016/j.ymben.2019.04.010. [PubMed: 31029860]

Abernathy MH, Yu J, Ma F, Liberton M, Ungerer J, Hollinshead WD, Gopalakrishnan S, He L, Maranas CD, Pakrasi HB, Allen DK, Tang YJ, 2017. Deciphering cyanobacterial phenotypes for fast photoautotrophic growth via isotopically nonstationary metabolic flux analysis. Biotechnol. Biofuels 10, 273. 10.1186/s13068-017-0958-y. [PubMed: 29177008]

Allen DK, 2016a. Assessing compartmentalized flux in lipid metabolism with isotopes. Biochim. Biophys. Acta Mol. Cell Biol. Lipids 1861, 1226–1242. 10.1016/j.bbalip.2016.03.017.

Allen DK, 2016b. Quantifying plant phenotypes with isotopic labeling & metabolic flux analysis. Curr. Opin. Biotechnol. 37, 45–52. 10.1016/j.copbio.2015.10.002. [PubMed: 26613198]

Allen DK, Bates PD, Tjellström H, 2015. Tracking the metabolic pulse of plant lipid production with isotopic labeling and flux analyses: past, present and future. Prog. Lipid Res. 58, 97–120. 10.1016/j.plipres.2015.02.002. [PubMed: 25773881]

Allen DK, Ohlrogge JB, Shachar-Hill Y, 2009. The role of light in soybean seed filling metabolism. Plant J. 58, 220–234. 10.1111/j.1365-313X.2008.03771.x. [PubMed: 19077167]

Allen DK, Young JD, 2020. Tracing metabolic flux through time and space with isotope labeling experiments. Curr. Opin. Biotechnol. 64, 92–100. 10.1016/j.copbio.2019.11.003. [PubMed: 31864070]

Allen DK, Young JD, 2013. Carbon and nitrogen provisions alter the metabolic flux in developing soybean embryos. Plant Physiol. 161, 1458–1475. 10.1104/pp.112.203299. [PubMed: 23314943]

Andrianov V, Borisjuk N, Pogrebnyak N, Brinker A, Dixon J, Spitsin S, Flynn J, Matyszczuk P, Andryszak K, Laurelli M, Golovkin M, Koprowski H, 2010. Tobacco as a production platform for biofuel: overexpression of Arabidopsis DGAT and LEC2 genes increases accumulation and shifts the composition of lipids in green biomass. Plant Biotechnol. J. 8, 277–287. 10.1111/j.1467-7652.2009.00458.x. [PubMed: 20051035]

Arisz SA, Heo J-Y, Koevoets IT, Zhao T, van Egmond P, Meyer AJ, Zeng W, Niu X, Wang B, Mitchell-Olds T, Schranz ME, Testerink C, 2018. DIACYLGLYCEROL ACYLTRANSFERASE1 contributes to freezing tolerance. Plant Physiol. 177 10.1104/pp.18.00503, 1410 LP–1424. [PubMed: 29907701]

Arp WJ, 1991. Effects of source-sink relations on photosynthetic acclimation to elevated CO2. Plant Cell Environ. 14, 869–875. 10.1111/j.1365-3040.1991.tb01450.x.

Arrivault S, Obata T, Szecówka M, Mengin V, Guenther M, Hoehne M, Fernie AR, Stitt M, 2016. Metabolite pools and carbon flow during C4 photosynthesis in maize: 13CO2 labeling kinetics and cell type fractionation. J. Exp. Bot. 68, 283–298. 10.1093/jxb/erw414. [PubMed: 27834209]

Baerenfaller K, Massonnet C, Hennig L, Russenberger D, Sulpice R, Walsh S, Stitt M, Granier C, Gruissem W, 2015. A long photoperiod relaxes energy management in Arabidopsis leaf six. Curr. Plant Biol. 2, 34–45. 10.1016/j.cpb.2015.07.001.

Bassham JA, Benson AA, Kay LD, Harris AZ, Wilson AT, Calvin M, 1954. The path of carbon in photosynthesis. XXI. The cyclic regeneration of carbon dioxide acceptor. J. Am. Chem. Soc. 76, 1760–1770. 10.1021/ja01636a012.

Baud S, 2018. Seeds as oil factories. Plant Reprod. 31, 213–235. 10.1007/s00497-018-0325-6. [PubMed: 29429143]

Baud S, Lepiniec L, 2010. Physiological and developmental regulation of seed oil production. Prog. Lipid Res. 49, 235–249. 10.1016/j.plipres.2010.01.001. [PubMed: 20102727]

Baud S, Wuillème S, To A, Rochat C, Lepiniec L, 2009. Role of WRINKLED1 in the transcriptional regulation of glycolytic and fatty acid biosynthetic genes in Arabidopsis. Plant J. 60, 933–947. 10.1111/j.1365-313X.2009.04011.x. [PubMed: 19719479]

Beechey-Gradwell Z, Cooney L, Winichayakul S, Andrews M, Hea SY, Crowther T, Roberts N, 2019. Storing carbon in leaf lipid sinks enhances perennial ryegrass carbon capture especially under high N and elevated CO2. J. Exp. Bot. 71, 2351–2361. 10.1093/jxb/erz494.

Bellasio C, Burgess SJ, Griffiths H, Hibberd JM, 2014. A high throughput gas exchange screen for determining rates of photorespiration or regulation of C4 activity. J. Exp. Bot. 65, 3769–3779. 10.1093/jxb/eru238. [PubMed: 25006037]

Bernacchi CJ, Singsaas EL, Pimentel C, Portis AR Jr., Long SP, 2001. Improved temperature response functions for models of Rubisco-limited photosynthesis. Plant Cell Environ. 24, 253–259. 10.1111/j.1365-3040.2001.00668.x.

Bourgis F, Kilaru A, Cao X, Ngando-Ebongue G-F, Drira N, Ohlrogge JB, Arondel V, 2011. Comparative transcriptome and metabolite analysis of oil palm and date palm mesocarp that differ dramatically in carbon partitioning. Proc. Natl. Acad. Sci. Unit. States Am. 108 10.1073/pnas.1106502108, 12527 LP–12532.

Bräutigam A, Schlüter U, Lundgren MR, Flachbart S, Ebenhöh O, Schönknecht G, Christin PA, Bleuler S, Droz JM, Osborne CP, Weber APM, Gowik U, 2018. Biochemical mechanisms driving rapid fluxes in C4 photosynthesis. bioRxiv, 387431. 10.1101/387431.

Browse J, Roughan PG, Slack CR, 1981. Light control of fatty acid synthesis and diurnal fluctuations of fatty acid composition in leaves. Biochem. J. 196, 347–354. 10.1042/bj1960347. [PubMed: 7197927]

Brugière N, Dubois F, Limami AM, Lelandais M, Roux Y, Sangwan RS, Hirel B, 1999. Glutamine synthetase in the phloem plays a major role in controlling proline production. Plant Cell 11, 1995–2011. 10.1105/tpc.11.10.1995. [PubMed: 10521528]

Cai Y, Whitehead P, Chappell J, Chapman KD, 2019. Mouse lipogenic proteins promote the co-accumulation of triacylglycerols and sesquiterpenes in plant cells. Planta 250, 79–94. 10.1007/s00425-019-03148-9. [PubMed: 30919065]

Cernac A, Benning C, 2004. WRINKLED1 encodes an AP2/EREB domain protein involved in the control of storage compound biosynthesis in Arabidopsis. Plant J. 40, 575–585. 10.1111/j.1365-313X.2004.02235.x. [PubMed: 15500472]

Cocuron JC, Koubaa M, Kimmelfield R, Ross Z, Alonso AP, 2019. A combined metabolomics and fluxomics analysis identifies steps limiting oil synthesis in Maize Embryos. Plant Physiol. 181, 961–975. 10.1104/PP.19.00920. [PubMed: 31530627]

Czajka JJ, Kambhampati S, Tang YJ, Wang Y, Allen DK, 2020. Application of stable isotope tracing to Elucidate metabolic dynamics during Yarrowia lipolytica α-Ionone fermentation. iScience 23, 100854. 10.1016/j.isci.2020.100854. [PubMed: 32058965]

Czedik-Eysenberg A, Arrivault S, Lohse MA, Feil R, Krohn N, Encke B, Nunes-Nesi A, Fernie AR, Lunn JE, Sulpice R, Stitt M, 2016. The interplay between carbon availability and growth in different zones of the growing maize leaf. Plant Physiol. 172, 943–967. 10.1104/pp.16.00994. [PubMed: 27582314]

Deerinck TJ, Shone TM, Bushong EA, Ramachandra R, Peltier ST, Ellisman MH, 2018. High-performance serial block-face SEM of nonconductive biological samples enabled by focal gas injection-based charge compensation. J. Microsc. 270, 142–149. 10.1111/jmi.12667. [PubMed: 29194648]

Ding B, Parthasarathy MV, Niklas K, Turgeon R, 1988. A morphometric analysis of the phloem-unloading pathway in developing tobacco leaves. Planta 176, 307–318. 10.1007/BF00395411. [PubMed: 24220859]

Durrett TP, Benning C, Ohlrogge J, 2008. Plant triacylglycerols as feedstocks for the production of biofuels. Plant J. 54, 593–607. 10.1111/j.1365-313X.2008.03442.x. [PubMed: 18476866]

Facchinelli F, Weber APM, 2011. The metabolite transporters of the plastid envelope: an update. Front. Plant Sci. 10.3389/fpls.2011.00050.

Fan J, Yan C, Roston R, Shanklin J, Xu C, 2014. Arabidopsis lipins, PDAT1 acyltransferase, and SDP1 triacylglycerol lipase synergistically direct fatty acids toward β-oxidation, thereby maintaining membrane lipid homeostasis. Plant Cell 26. 10.1105/tpc.114.130377, 4119 LP–4134. [PubMed: 25293755]

Fan J, Yu L, Xu C, 2017. A central role for triacylglycerol in membrane lipid breakdown, fatty acid β-oxidation, and plant survival under extended darkness. Plant Physiol. 174 10.1104/pp.17.00653, 1517 LP–1530. [PubMed: 28572457]

Fatland B, Anderson M, Nikolau BJ, Wurtele ES, 2000. Molecular biology of cytosolic acetyl-CoA generation. Biochem. Soc. Trans. 28, 593–595. 10.1042/bst0280593. [PubMed: 11171137]

Fatland BL, Ke J, Anderson MD, Mentzen WI, Cui LW, Allred CC, Johnston JL, Nikolau BJ, Wurtele ES, 2002. Molecular characterization of a heteromeric ATP-citrate lyase that generates cytosolic acetyl-coenzyme A in arabidopsis. Plant Physiol. 130 10.1104/pp.008110, 740 LP–756. [PubMed: 12376641]

Fernandez CA, Des Rosiers C, Previs SF, David F, Brunengraber H, 1996. Correction of 13C mass isotopomer distributions for natural stable isotope abundance. J. Mass Spectrom. 31, 255–262. 10.1002/(SICI)1096-9888(199603)31:3<255::AID-JMS290>3.0.CO;2-3. [PubMed: 8799277]

Fernandez O, Ishihara H, George GM, Mengin V, Flis A, Sumner D, Arrivault S, Feil R, Lunn JE, Zeeman SC, Smith AM, Stitt M, 2017. Leaf starch turnover occurs in long days and in falling light at the end of the day. Plant Physiol. 174, 2199–2212. 10.1104/pp.17.00601. [PubMed: 28663333]

Fondy BR, Geiger DR, 1982. Diurnal pattern of translocation and carbohydrate metabolism in source leaves of *Beta vulgaris* L. Plant Physiol. 70, 671–676. 10.1104/pp.70.3.671. [PubMed: 16662555]

Geiger DR, Servaites JC, 1994. Diurnal regulation of photosynthetic carbon metabolism in C3 plants. Annu. Rev. Plant Physiol. Plant Mol. Biol. 45, 235–256. 10.1146/annurev.pp.45.060194.001315.

Gerrard Wheeler MC, Arias CL, Righini S, Badia MB, Andreo CS, Drincovich MF, Saigo M, 2016. Differential contribution of malic enzymes during soybean and castor seeds maturation. PLoS One 11. 10.1371/journal.pone.0158040 e0158040–e0158040. [PubMed: 27347875]

Gibon Y, Pyl ET, Sulpice R, Lunn JE, HÖhne M, GÜnther M, Stitt M, 2009. Adjustment of growth, starch turnover, protein content and central metabolism to a decrease of the carbon supply when Arabidopsis is grown in very short photoperiods. Plant Cell Environ. 32, 859–874. 10.1111/j.1365-3040.2009.01965.x. [PubMed: 19236606]

Goldschmidt EE, Huber SC, 1992. Regulation of photosynthesis by end-product accumulation in leaves of plants storing starch, sucrose, and hexose sugars. Plant Physiol. 99, 1443–1448. 10.1104/pp.99.4.1443. [PubMed: 16669056]

Graf A, Schlereth A, Stitt M, Smith AM, 2010. Circadian control of carbohydrate availability for growth in Arabidopsis plants at night. Proc. Natl. Acad. Sci. U.S.A. 107, 9458–9463. 10.1073/pnas.0914299107. [PubMed: 20439704]

Graf A, Smith AM, 2011. Starch and the clock: the dark side of plant productivity. Trends Plant Sci. 16, 169–175. 10.1016/j.tplants.2010.12.003. [PubMed: 21216654]

Grimmer C, Bachfischer T, Komor E, 1999. Carbohydrate partitioning into starch in leaves of Ricinus communis L. grown under elevated CO2 is controlled by sucrose. Plant Cell Environ. 22, 1275–1280. 10.1046/j.1365-3040.1999.00481.x.

Gu H, Liu G, Wang J, Aubry AF, Arnold ME, 2014. Selecting the correct weighting factors for linear and quadratic calibration curves with least-squares regression algorithm in bioanalytical LC-MS/MS assays and impacts of using incorrect weighting factors on curve stability, data quality, and assay perfo. Anal. Chem. 86, 8959–8966. 10.1021/ac5018265. [PubMed: 25157966]

Hädrich N, Hendriks JHM, Kötting O, Arrivault S, Feil R, Zeeman SC, Gibon Y, Schulze WX, Stitt M, Lunn JE, 2012. Mutagenesis of cysteine 81 prevents dimerization of the APS1 subunit of ADP-glucose pyrophosphorylase and alters diurnal starch turnover in Arabidopsis thaliana leaves. Plant J. 70, 231–242. 10.1111/j.1365-313X.2011.04860.x. [PubMed: 22098298]

Hasunuma T, Harada K, Miyazawa SI, Kondo A, Fukusaki E, Miyake C, 2010. Metabolic turnover analysis by a combination of in vivo 13C-labelling from 13CO2 and metabolic profiling with CE-MS/MS reveals rate-limiting steps of the C3 photosynthetic pathway in Nicotiana tabacum leaves. J. Exp. Bot. 61, 1041–1051. 10.1093/jxb/erp374. [PubMed: 20026474]

Häusler RE, Schlieben NH, Schulz B, Flügge UI, 1998. Compensation of decreased triose phosphate/phosphate translocator activity by accelerated starch turnover and glucose transport in transgenic tobacco. Planta 204, 366–376. 10.1007/s004250050268. [PubMed: 9530880]

Hendry JI, Prasannan C, Ma F, Möllers KB, Jaiswal D, Digmurti M, Allen DK, Frigaard NU, Dasgupta S, Wangikar PP, 2017. Rerouting of carbon flux in a glycogen mutant of cyanobacteria assessed via isotopically non-stationary 13C metabolic flux analysis. Biotechnol. Bioeng. 114, 2298–2308. 10.1002/bit.26350. [PubMed: 28600876]

Hibberd JM, Quick WP, 2002. Characteristics of C4 photosynthesis in stems and petioles of C3 flowering plants. Nature 415, 451–454. 10.1038/415451a. [PubMed: 11807559]

Hocking PJ, 1980. The composition of phloem exudate and xylem sap from tree tobacco (Nicotiana glauca Grah.). Ann. Bot. 45, 633–643. 10.1093/oxfordjournals.aob.a085871.

Hua Y, Laserstein P, Helmstaedter M, 2015. Large-volume en-bloc staining for electron microscopy-based connectomics. Nat. Commun. 6, 7923. 10.1038/ncomms8923. [PubMed: 26235643]

Huang AHC, 1996. Oleosins and oil bodies in seeds and other organs. Plant Physiol. 110, 1055–1061. 10.1104/pp.110.4.1055. [PubMed: 8934621]

Huber SC, 1989. Biochemical mechanism for regulation of sucrose accumulation in leaves during photosynthesis. Plant Physiol. 91, 656–662. 10.1104/pp.91.2.656. [PubMed: 16667083]

Ischebeck T, Krawczyk HE, Mullen RT, Dyer JM, Chapman KD, 2020. Lipid droplets in plants and algae: distribution, formation, turnover and function. Semin. Cell Dev. Biol. 10.1016/j.semcdb.2020.02.014.

Jako C, Kumar A, Wei Y, Zou J, Barton DL, Giblin EM, Covello PS, Taylor DC, 2001. Seed-specific over-expression of an arabidopsis cDNA encoding a diacylglycerol acyltransferase enhances seed oil content and seed weight. Plant Physiol. 126, 861–874. 10.1104/pp.126.2.861. [PubMed: 11402213]

Jenkins LM, Nam JW, Evans BS, Allen DK, 2021. Quantification of Acyl-Acyl Carrier Proteins for Fatty Acid Synthesis Using LC-MS/MS. In: Bartels D, Dörmann P (Eds.), Methods in Molecular Biology. Springer US, New York, NY, pp. 219–247. 10.1007/978-1-0716-1362-7_13.

Kalt-Torres W, Huber SC, 1987. Diurnal changes in maize leaf photosynthesis. Plant Physiol. 83, 294–298. 10.1104/pp.83.2.294. [PubMed: 16665239]

Kambhampati S, Li J, Evans BS, Allen DK, 2019. Accurate and efficient amino acid analysis for protein quantification using hydrophilic interaction chromatography coupled tandem mass spectrometry. Plant Methods 15, 46. 10.1186/s13007-019-0430-z. [PubMed: 31110556]

Kang F, Rawsthorne S, 1994. Starch and fatty acid synthesis in plastids from developing embryos of oilseed rape (Brassica napus L.). Plant J. 6, 795–805. 10.1046/j.1365-313X.1994.6060795.x.

Kaup MT, Froese CD, Thompson JE, 2002. A role for diacylglycerol acyltransferase during leaf senescence. Plant Physiol. 129, 1616–1626. 10.1104/pp.003087. [PubMed: 12177474]

Kelly AA, van Erp HV, Quettier AL, Shaw E, Menard G, Kurup S, Eastmond PJ, 2013. The SUGAR-DEPENDENT1 lipase limits triacylglycerol accumulation in vegetative tissues of Arabidopsis. Plant Physiol. 162, 1282–1289. 10.1104/pp.113.219840. [PubMed: 23686420]

Koiwai A, Suzuki F, Matsuzaki T, Kawashima N, 1983. The fatty acid composition of seeds and leaves of Nicotiana species. Phytochemistry 22, 1409–1412. 10.1016/S0031-9422(00)84024-8.

Konarska A, Łotocka B, 2020. Glandular trichomes of Robinia viscosa Vent. var. hartwigii (Koehne) Ashe (Faboideae, Fabaceae)—morphology, histochemistry and ultrastructure. Planta 252, 102. 10.1007/s00425-020-03513-z. [PubMed: 33180181]

Laterre R, Pottier M, Remacle C, Boutry M, 2017. Photosynthetic trichomes contain a specific rubisco with a modified pH-dependent activity. Plant Physiol. 173, 2110–2120. 10.1104/pp.17.00062. [PubMed: 28250069]

Lauxmann MA, Annunziata MG, Brunoud G, Wahl V, Koczut A, Burgos A, Olas JJ, Maximova E, Abel C, Schlereth A, Soja AM, Bläsing OE, Lunn JE, Vernoux T, Stitt M, 2016. Reproductive failure in Arabidopsis thaliana under transient carbohydrate limitation: flowers and very young siliques are jettisoned and the meristem is maintained to allow successful resumption of reproductive growth. Plant Cell Environ. 39, 745–767. 10.1111/pce.12634. [PubMed: 26351840]

Li-Beisson Y, Shorrosh B, Beisson F, Andersson MX, Arondel V, Bates PD, Baud S, Bird D, DeBono A, Durrett TP, Franke RB, Graham IA, Katayama K, Kelly AA, Larson T, Markham JE, Miquel M, Molina I, Nishida I, Rowland O, Samuels L, Schmid KM, Wada H, Welti R, Xu C, Zallot R, Ohlrogge J, 2013. Acyl-lipid metabolism. Arab. B. 11, e0161 10.1199/tab.0161.

Lonien J, Schwender J, 2009. Analysis of metabolic flux phenotypes for two arabidopsis mutants with severe impairment in seed storage lipid synthesis. Plant Physiol. 151, 1617–1634. 10.1104/pp.109.144121. [PubMed: 19755540]

Lorenzen JH, Ewing EE, 1992. Starch accumulation in leaves of potato (Solarium tuberosum l.) during the first 18 days of photoperiod treatment. Ann. Bot. 69, 481–485. 10.1093/oxfordjournals.aob.a088375.

Lu Y, Gehan JP, Sharkey TD, 2005. Daylength and circadian effects on starch degradation and maltose metabolism. Plant Physiol. 138, 2280–2291. 10.1104/pp.105.061903. [PubMed: 16055686]

Ludewig F, Flügge UI, 2013. Role of metabolite transporters in source-sink carbon allocation. Front. Plant Sci. 10.3389/fpls.2013.00231.

Ma F, Jazmin LJ, Young JD, Allen DK, 2017. Isotopically Nonstationary Metabolic Flux Analysis (INST-MFA) of Photosynthesis and Photorespiration in Plants. In: Fernie AR, Bauwe H, Weber APM (Eds.), Methods in Molecular Biology. Springer New York, New York, NY, pp. 167–194. 10.1007/978-1-4939-7225-8_12.

Ma F, Jazmin LJ, Young JD, Allen DK, 2014. Isotopically nonstationary 13C flux analysis of changes in Arabidopsis thaliana leaf metabolism due to high light acclimation. Proc. Natl. Acad. Sci. U.S.A. 111, 16967–16972. 10.1073/pnas.1319485111. [PubMed: 25368168]

Masakapalli SK, Kruger NJ, Ratcliffe RG, 2013. The metabolic flux phenotype of heterotrophic Arabidopsis cells reveals a complex response to changes in nitrogen supply. Plant J. 74, 569–582. 10.1111/tpj.12142. [PubMed: 23406511]

Masakapalli SK, Ritala A, Dong L, Van Der Krol AR, Oksman-Caldentey KM, Ratcliffe RG, Sweetlove LJ, 2014. Metabolic flux phenotype of tobacco hairy roots engineered for increased geraniol production. Phytochemistry 99, 73–85. 10.1016/j.phytochem.2013.12.007. [PubMed: 24472392]

Matheson N, Wheatley J, 1963. Diurnal-nocturnal changes in the starch of tobacco leaves. Aust. J. Biol. Sci. 16, 70. 10.1071/bi9630070.

Matt P, Schurr U, Klein D, Krapp A, Stitt M, 1998. Growth of tobacco in short-day conditions leads to high starch, low sugars, altered diurnal changes in the Nia transcript and low nitrate reductase activity, and inhibition of amino acid synthesis. Planta 207, 27–41. 10.1007/s004250050452. [PubMed: 9951717]

McClain AM, Sharkey TD, 2019. Triose phosphate utilization and beyond: from photosynthesis to end product synthesis. J. Exp. Bot. 70, 1755–1766. 10.1093/jxb/erz058. [PubMed: 30868155]

McCleary BV, Charmier LMJ, McKie VA, 2019. Measurement of starch: critical Evaluation of current methodology. Starch Staerke 71, 1800146. 10.1002/star.201800146.

McCleary BV, Gibson TS, Mugford DC, 1997. Measurement of total starch in cereal products by amyloglucosidase-α-amylase method: collaborative study. J. AOAC Int. 80, 571–579. 10.1093/jaoac/80.3.571.

Mengin V, Pyl ET, Moraes TA, Sulpice R, Krohn N, Encke B, Stitt M, 2017. Photosynthate partitioning to starch in arabidopsis thaliana is insensitive to light intensity but sensitive to

photoperiod due to a restriction on growth in the light in short photoperiods. Plant Cell Environ. 40, 2608–2627. 10.1111/pce.13000. [PubMed: 28628949]

Mitchell MC, Pritchard J, Okada S, Zhang J, Venables I, Vanhercke T, Ral J, 2020. Increasing growth and yield by altering carbon metabolism in a transgenic leaf oil crop. Plant Biotechnol. 10.1111/pbi.13363. J. n/a, pbi.13363.

Miyake H, 2016. Starch accumulation in the bundle sheaths of C3 plants: a possible precondition for C4 photosynthesis. Plant Cell Physiol. 57, 890–896. 10.1093/pcp/pcw046. [PubMed: 26936788]

Miyake H, Maeda E, 1976. Development of bundle sheath chloroplasts in rice seedlings. Can. J. Bot. 54, 556–565. 10.1139/b76-056.

Moore BD, Cheng SH, Rice J, Seemann JR, 1998. Sucrose cycling, Rubisco expression, and prediction of photosynthetic acclimation to elevated atmospheric CO2. Plant Cell Environ. 21, 905–915. 10.1046/j.1365-3040.1998.00324.x.

Moore BD, Palmquist DE, Seemann JR, 1997. Influence of plant growth at high CO2 concentrations on leaf content of ribulose-1,5-bisphosphate carboxylase/oxygenase and intracellular distribution of soluble carbohydrates in tobacco, snapdragon, and parsley. Plant Physiol. 115, 241–248. 10.1104/pp.115.1.241. [PubMed: 12223804]

Morcuende R, Bari R, Gibon Y, Zheng W, Pant BD, Bläsing O, Usadel B, Czechowski T, Udvardi MK, Stitt M, Scheible WR, 2007. Genome-wide reprogramming of metabolism and regulatory networks of Arabidopsis in response to phosphorus. Plant Cell Environ. 30, 85–112. 10.1111/j.1365-3040.2006.01608.x. [PubMed: 17177879]

Müller GL, Drincovich MF, Andreo CS, Lara MV, 2008. Nicotiana tabacum NADP-malic enzyme: cloning, characterization and analysis of biological role. Plant Cell Physiol. 49, 469–480. 10.1093/pcp/pcn022. [PubMed: 18272530]

Nam JW, Jenkins LM, Li J, Evans BS, Jaworski JG, Allen DK, 2020. A general method for quantification and discovery of acyl groups attached to acyl carrier proteins in fatty acid metabolism using LC-MS/MS. Plant Cell 32, 820–832. 10.1105/tpc.19.00954. [PubMed: 32060179]

Niittylä T, Messerli G, Trevisan M, Chen J, Smith AM, Zeeman SC, 2004. A previously unknown maltose transporter essential for starch degradation in leaves. Science (80-.) 303. 10.1126/science.1091811, 87 LP–89.

Parajuli S, Kannan B, Karan R, Sanahuja G, Liu H, Garcia-Ruiz E, Kumar D, Singh V, Zhao H, Long S, Shanklin J, Altpeter F, 2020. Towards oilcane: engineering hyperaccumulation of triacylglycerol into sugarcane stems. GCB Bioenergy n/a. 10.1111/gcbb.12684.

Pilkington SM, Encke B, Krohn N, Höhne M, Stitt M, Pyl ET, 2015. Relationship between starch degradation and carbon demand for maintenance and growth in Arabidopsis thaliana in different irradiance and temperature regimes. Plant Cell Environ. 38, 157–171. 10.1111/pce.12381. [PubMed: 24905937]

Prabhakar V, Löttgert T, Gigolashvili T, Bell K, Flügge UI, Häusler RE, 2009. Molecular and functional characterization of the plastid-localized Phosphoenolpyruvate enolase (ENO1) from Arabidopsis thaliana. FEBS Lett. 583, 983–991. 10.1016/j.febslet.2009.02.017. [PubMed: 19223001]

Raines CA, Paul MJ, 2006. Products of leaf primary carbon metabolism modulate the developmental programme determining plant morphology. J. Exp. Bot. 57, 1857–1862. 10.1093/jxb/erl011. [PubMed: 16714302]

Rangasamy D, Ratledge C, 2000. Compartmentation of ATP:citrate lyase in plants. Plant Physiol. 122, 1225–1230. 10.1104/pp.122.4.1225. [PubMed: 10759519]

Ratcliffe RG, Shachar-Hill Y, 2006. Measuring multiple fluxes through plant metabolic networks. Plant J. 45, 490–511. 10.1111/j.1365-313X.2005.02649.x. [PubMed: 16441345]

Routaboul JM, Benning C, Bechtold N, Caboche M, Lepiniec L, 1999. The TAG11 locus of Arabidopsis encodes for a diacylglycerol acyltransferase. Plant Physiol. Biochem. 37, 831–840. 10.1016/S0981-9428(99)00115-1. [PubMed: 10580283]

Ruckle ME, Meier MA, Frey L, Eicke S, Kölliker R, Zeeman SC, Studer B, 2017. Diurnal leaf starch content: an orphan trait in forage legumes. Agronomy 7, 16.

Rufty TW, Huber SC, Volk RJ, 1988. Alterations in leaf carbohydrate metabolism in response to nitrogen stress. Plant Physiol. 88, 725–730. 10.1104/pp.88.3.725. [PubMed: 16666374]

Sanjaya, Durrett TP, Weise SE, Benning C, 2011. Increasing the energy density of vegetative tissues by diverting carbon from starch to oil biosynthesis in transgenic Arabidopsis. Plant Biotechnol. J. 9, 874–883. 10.1111/j.1467-7652.2011.00599.x. [PubMed: 22003502]

Santos Mendoza M, Dubreucq B, Miquel M, Caboche M, Lepiniec L, 2005. LEAFY COTYLEDON 2 activation is sufficient to trigger the accumulation of oil and seed specific mRNAs in Arabidopsis leaves. FEBS Lett. 579, 4666–4670. 10.1016/j.febslet.2005.07.037. [PubMed: 16107256]

Sasaki Y, Kozaki A, Hatano M, 1997. Link between light and fatty acid synthesis: thioredoxin-linked reductive activation of plastidic acetyl-CoA carboxylase. Proc. Natl. Acad. Sci. U.S.A. 94, 11096–11101. 10.1073/pnas.94.20.11096. [PubMed: 9380765]

Sauer A, Heise K-P, 1984. Regulation of acetyl-coenzyme A carboxylase and acetyl-coenzyme A synthetase in spinach chloroplasts. Zeitschrift für Naturforsch. C 39, 268–275. 10.1515/znc-1984-3-412.

Schwender J, Hebbelmann I, Heinzel N, Hildebrandt T, Rogers A, Naik D, Klapperstück M, Braun HP, Schreiber F, Denolf P, Borisjuk L, Rolletschek H, 2015. Quantitative multilevel analysis of central metabolism in developing oilseeds of oilseed rape during in vitro culture. Plant Physiol. 168, 828–848. 10.1104/pp.15.00385. [PubMed: 25944824]

Scialdone A, Mugford ST, Feike D, Skeffngton A, Borrill P, Graf A, Smith AM, Howard M, 2013. Arabidopsis plants perform arithmetic division to prevent starvation at night. Elife, e00669. 10.7554/eLife.00669, 2013.

Scott RW, Winichayakul S, Roldan M, Cookson R, Willingham M, Castle M, Pueschel R, Peng CC, Tzen JTC, Roberts NJ, 2010. Elevation of oil body integrity and emulsion stability by polyoleosins, multiple oleosin units joined in tandem head-to-tail fusions. Plant Biotechnol. J. 8, 912–927. 10.1111/j.1467-7652.2010.00522.x. [PubMed: 20444209]

Sharkey TD, Berry JA, Raschke K, 1985. Starch and sucrose synthesis in Phaseolus vulgaris as affected by light, CO 2, and abscisic acid. Plant Physiol. 77, 617–620. 10.1104/pp.77.3.617. [PubMed: 16664108]

Sharkey TD, Preiser AL, Weraduwage SM, Gog L, 2020. Source of 12C in Calvin Benson cycle intermediates and isoprene emitted from plant leaves fed with 13CO2. Biochem. J. 10.1042/bcj20200480.

Sharkey TD, Weise SE, 2016. The glucose 6-phosphate shunt around the Calvin-Benson cycle. J. Exp. Bot. 67, 4067–4077. 10.1093/jxb/erv484. [PubMed: 26585224]

Shastri AA, Morgan JA, 2007. A transient isotopic labeling methodology for 13C metabolic flux analysis of photoautotrophic microorganisms. Phytochemistry 68, 2302–2312. 10.1016/j.phytochem.2007.03.042. [PubMed: 17524438]

Slocombe SP, Cornah J, Pinfield-Wells H, Soady K, Zhang Q, Gilday A, Dyer JM, Graham IA, 2009. Oil accumulation in leaves directed by modification of fatty acid breakdown and lipid synthesis pathways. Plant Biotechnol. J. 7, 694–703. 10.1111/j.1467-7652.2009.00435.x. [PubMed: 19702756]

Smith AM, Stitt M, 2007. Coordination of carbon supply and plant growth. Plant Cell Environ. 30, 1126–1149. 10.1111/j.1365-3040.2007.01708.x. [PubMed: 17661751]

Smith AM, Zeeman SC, 2020. Starch: a flexible, adaptable carbon store coupled to plant growth. Annu. Rev. Plant Biol. 1–29. 10.1146/annurev-arplant-050718-100241. [PubMed: 32197053]

Smith RG, Gauthier DA, Dennis DT, Turpin DH, 1992. Malate- and pyruvate-dependent fatty acid synthesis in leucoplasts from developing castor endosperm. Plant Physiol. 98, 1233–1238. 10.1104/pp.98.4.1233. [PubMed: 16668781]

Stitt M, Ap Rees T, 1979. Capacities of pea chloroplasts to catalyse the oxidative pentose phosphate pathway and glycolysis. Phytochemistry 18, 1905–1911. 10.1016/S0031-9422(00)82700-4.

Stitt M, Gerhardt R, Kürzel B, Heldt HW, 1983. A role for fructose 2,6-bisphosphate in the regulation of sucrose synthesis in spinach leaves. Plant Physiol. 72 10.1104/pp.72.4.1139, 1139 LP–1141. [PubMed: 16663136]

Stitt M, Quick WP, 1989. Photosynthetic carbon partitioning: its regulation and possibilities for manipulation. Physiol. Plantarum 77, 633–641. 10.1111/j.1399-3054.1989.tb05402.x.

Stitt M, Zeeman SC, 2012. Starch turnover: pathways, regulation and role in growth. Curr. Opin. Plant Biol. 15, 282–292. 10.1016/j.pbi.2012.03.016. [PubMed: 22541711]

Stone SL, Kwong LW, Yee KM, Pelletier J, Lepiniec L, Fischer RL, Goldberg RB, Harada JJ, 2001. LEAFY COTYLEDON2 encodes a B3 domain transcription factor that induces embryo development. Proc. Natl. Acad. Sci. U.S.A. 98, 11806–11811. 10.1073/pnas.201413498. [PubMed: 11573014]

Stuhlfauth T, Scheuermann R, Fock HP, 1990. Light energy dissipation under water stress conditions: contribution of reassimilation and evidence for additional processes. Plant Physiol. 92, 1053–1061. 10.1104/pp.92.4.1053. [PubMed: 16667370]

Stutz SS, Hanson DT, 2019. Contribution and consequences of xylem-transported CO2 assimilation for C3 plants. New Phytol. 223, 1230–1240. 10.1111/nph.15907. [PubMed: 31081546]

Sulpice R, Flis A, Ivakov AA, Apelt F, Krohn N, Encke B, Abel C, Feil R, Lunn JE, Stitt M, 2014. Arabidopsis coordinates the diurnal regulation of carbon allocation and growth across a wide range of Photoperiods. Mol. Plant 7, 137–155. 10.1093/mp/sst127. [PubMed: 24121291]

Szecowka M, Heise R, Tohge T, Nunes-Nesi A, Vosloh D, Huege J, Feil R, Lunn J, Nikoloski Z, Stitt M, Fernie AR, Arrivault S, 2013. Metabolic fluxes in an illuminated arabidopsis rosette. Plant Cell 25. 10.1105/tpc.112.106989, 694 LP–714. [PubMed: 23444331]

Tcherkez G, Mahé A, Gauthier P, Mauve C, Gout E, Bligny R, Cornic G, Hodges M, 2009. In folio respiratory fluxomics revealed by 13C isotopic labeling and H/D isotope effects highlight the noncyclic nature of the tricarboxylic acid “cycle” in illuminated leaves. Plant Physiol. 151, 620–630. 10.1104/pp.109.142976. [PubMed: 19675152]

Tsogtbaatar E, Cocuron JC, Alonso AP, 2020. Non-conventional pathways enable pennycress (Thlaspi arvense L.) embryos to achieve high efficiency of oil biosynthesis. J. Exp. Bot. 71, 3037–3051. 10.1093/jxb/eraa060. [PubMed: 32006014]

Turgeon R, 2006. Phloem loading: how leaves gain their independence. Bioscience 56, 15. 10.1641/0006-3568(2006)056[0015:plhlgt]2.0.co;2.

Turgeon R, Webb JA, 1976. Leaf development and phloem transport in Cucurbita pepo: Maturation of the minor veins. Planta 129, 265–269. 10.1007/BF00398269. [PubMed: 24430968]

Vanhercke T, Belide S, Taylor MC, El Tahchy A, Okada S, Rolland V, Liu Q, Mitchell M, Shrestha P, Venables I, Ma L, Blundell C, Mathew A, Ziolkowski L, Niesner N, Hussain D, Dong B, Liu G, Godwin ID, Lee J, Rug M, Zhou XR, Singh SP, Petrie JR, 2019a. Up-regulation of lipid biosynthesis increases the oil content in leaves of Sorghum bicolor. Plant Biotechnol. J. 17, 220–232. 10.1111/pbi.12959. [PubMed: 29873878]

Vanhercke T, Divi UK, El Tahchy A, Liu Q, Mitchell M, Taylor MC, Eastmond PJ, Bryant F, Mechanicos A, Blundell C, Zhi Y, Belide S, Shrestha P, Zhou XR, Ral JP, White RG, Green A, Singh SP, Petrie JR, 2017. Step changes in leaf oil accumulation via iterative metabolic engineering. Metab. Eng. 39, 237–246. 10.1016/j.ymben.2016.12.007. [PubMed: 27993560]

Vanhercke T, Dyer JM, Mullen RT, Kilaru A, Rahman MM, Petrie JR, Green AG, Yurchenko O, Singh SP, 2019b. Metabolic engineering for enhanced oil in biomass. Prog. Lipid Res. 74, 103–129. 10.1016/j.plipres.2019.02.002. [PubMed: 30822461]

Vanhercke T, El Tahchy A, Liu Q, Zhou XR, Shrestha P, Divi UK, Ral JP, Mansour MP, Nichols PD, James CN, Horn PJ, Chapman KD, Beaudoin F, Ruiz-López N, Larkin PJ, de Feyter RC, Singh SP, Petrie JR, 2014a. Metabolic engineering of biomass for high energy density: oilseed-like triacylglycerol yields from plant leaves. Plant Biotechnol. J. 12, 231–239. 10.1111/pbi.12131. [PubMed: 24151938]

Vanhercke T, El Tahchy A, Shrestha P, Zhou XR, Singh SP, Petrie JR, 2013. Synergistic effect of WRI1 and DGAT1 coexpression on triacylglycerol biosynthesis in plants. FEBS Lett. 587, 364–369. 10.1016/j.febslet.2012.12.018. [PubMed: 23313251]

Vanhercke T, Petrie JR, Singh SP, 2014b. Energy densification in vegetative biomass through metabolic engineering. Biocatal. Agric. Biotechnol. 3, 75–80. 10.1016/j.bcab.2013.11.010.

Vriet C, Welham T, Brachmann A, Marilyn PM, Pike J, Perry J, Parniske M, Sato S, Tabata S, Smith AM, Wang TL, 2010. A suite of Lotus japonicus starch mutants reveals both conserved and novel features of starch metabolism. Plant Physiol. 154, 643–655. 10.1104/pp.110.161844. [PubMed: 20699404]

Wagner GJ, 1991. Secreting glandular trichomes: more than just hairs. Plant Physiol. 96, 675–679. 10.1104/pp.96.3.675. [PubMed: 16668241]

Walker B, Ariza LS, Kaines S, Badger MR, Cousins AB, 2013. Temperature response of in vivoRubisco kinetics and mesophyll conductance in Arabidopsis thaliana: comparisons to Nicotiana tabacum. Plant Cell Environ. 36, 2108–2119. 10.1111/pce.12166. [PubMed: 23869820]

Weise SE, Weber APM, Sharkey TD, 2004. Maltose is the major form of carbon exported from the chloroplast at night. Planta 218, 474–482. 10.1007/s00425-003-1128-y. [PubMed: 14566561]

Weiszmann J, Fürtauer L, Weckwerth W, Nägele T, 2018. Vacuolar sucrose cleavage prevents limitation of cytosolic carbohydrate metabolism and stabilizes photosynthesis under abiotic stress. FEBS J. 285, 4082–4098. 10.1111/febs.14656. [PubMed: 30216682]

Weselake RJ, 2016. Engineering Oil Accumulation in Vegetative Tissue. In: Industrial Oil Crops., pp. 413–434. 10.1016/B978-1-893997-98-1.00015-4.

Weselake RJ, Taylor DC, Rahman MH, Shah S, Laroche A, McVetty PBE, Harwood JL, 2009. Increasing the flow of carbon into seed oil. Biotechnol. Adv. 27, 866–878. 10.1016/j.biotechadv.2009.07.001. [PubMed: 19625012]

Whitney SM, Sharwood RE, Orr D, White SJ, Alonso H, Galmés J, 2011. Isoleucine 309 acts as a C 4 catalytic switch that increases ribulose-1,5-bisphosphate carboxylase/oxygenase (rubisco) carboxylation rate in flaveria. Proc. Natl. Acad. Sci. U.S.A. 108, 14688–14693. 10.1073/pnas.1109503108. [PubMed: 21849620]

Winichayakul S, William Scott R, Roldan M, Bertrand Hatier JH, Livingston S, Cookson R, Curran AC, Roberts NJ, 2013. In vivo packaging of triacylglycerols enhances arabidopsis leaf biomass and energy density. Plant Physiol. 162, 626–639. 10.1104/pp.113.216820. [PubMed: 23616604]

Xu C, Shanklin J, 2016. Triacylglycerol metabolism, function, and accumulation in plant vegetative tissues. Annu. Rev. Plant Biol. 67, 179–206. 10.1146/annurev-arplant-043015-111641. [PubMed: 26845499]

Xu Y, Fu X, Sharkey TD, Shachar-Hill Y, Walker BJ, 2021. The metabolic origins of non-photorespiratory CO2 release during photosynthesis: a metabolic flux analysis. Plant Physiol. 10.1093/plphys/kiab076.

Yang Z, Ohlrogge JB, 2009. Turnover of fatty acids during natural senescence of arabidopsis, brachypodium, and switchgrass and in arabidopsis β-oxidation mutants. Plant Physiol. 150, 1981–1989. 10.1104/pp.109.140491. [PubMed: 19561121]

Ye Y, Nikovics K, To A, Lepiniec L, Fedosejevs ET, Van Doren SR, Baud S, Thelen JJ, 2020. Docking of acetyl-CoA carboxylase to the plastid envelope membrane attenuates fatty acid production in plants. Nat. Commun. 11 10.1038/s41467-020-20014-5.

Young JD, 2014. INCA: a computational platform for isotopically non-stationary metabolic flux analysis. Bioinformatics 30, 1333–1335. 10.1093/bioinformatics/btu015. [PubMed: 24413674]

Young JD, Shastri AA, Stephanopoulos G, Morgan JA, 2011. Mapping photoautotrophic metabolism with isotopically nonstationary 13C flux analysis. Metab. Eng. 13, 656–665. 10.1016/j.ymben.2011.08.002. [PubMed: 21907300]

Yu L, Fan J, Yan C, Xu C, 2018. Starch deficiency enhances lipid biosynthesis and turnover in leaves. Plant Physiol. 178, 118–129. 10.1104/pp.18.00539. [PubMed: 30076222]

Zale J, Jung JH, Kim JY, Pathak B, Karan R, Liu H, Chen X, Wu H, Candreva J, Zhai Z, Shanklin J, Altpeter F, 2016. Metabolic engineering of sugarcane to accumulate energy-dense triacylglycerols in vegetative biomass. Plant Biotechnol. J. 14, 661–669. 10.1111/pbi.12411. [PubMed: 26058948]

Zeeman SC, Kossmann J, Smith AM, 2010. Starch: its metabolism, Evolution, and biotechnological modification in plants. Annu. Rev. Plant Biol. 61, 209–234. 10.1146/annurev-arplant-042809-112301. [PubMed: 20192737]

Zhai Z, Liu H, Xu C, Shanklin J, 2017. Sugar potentiation of fatty acid and triacylglycerol accumulation. Plant Physiol. 175, 696–707. 10.1104/pp.17.00828. [PubMed: 28842550]

Zhou X-R, Bhandari S, Johnson BS, Kotapati HK, Allen DK, Vanhercke T, Bates PD, 2020. Reorganization of acyl flux through the lipid metabolic network in oil-accumulating tobacco leaves. Plant Physiol. 182 10.1104/pp.19.00667, 739 LP–755. [PubMed: 31792147]

Zou J, Wei Y, Jako C, Kumar A, Selvaraj G, Taylor DC, 1999. The Arabidopsis thaliana TAG1 mutant has a mutation in a diacylglycerol acyltransferase gene. Plant J. 19, 645–653. 10.1046/j.1365-313X.1999.00555.x. [PubMed: 10571850]

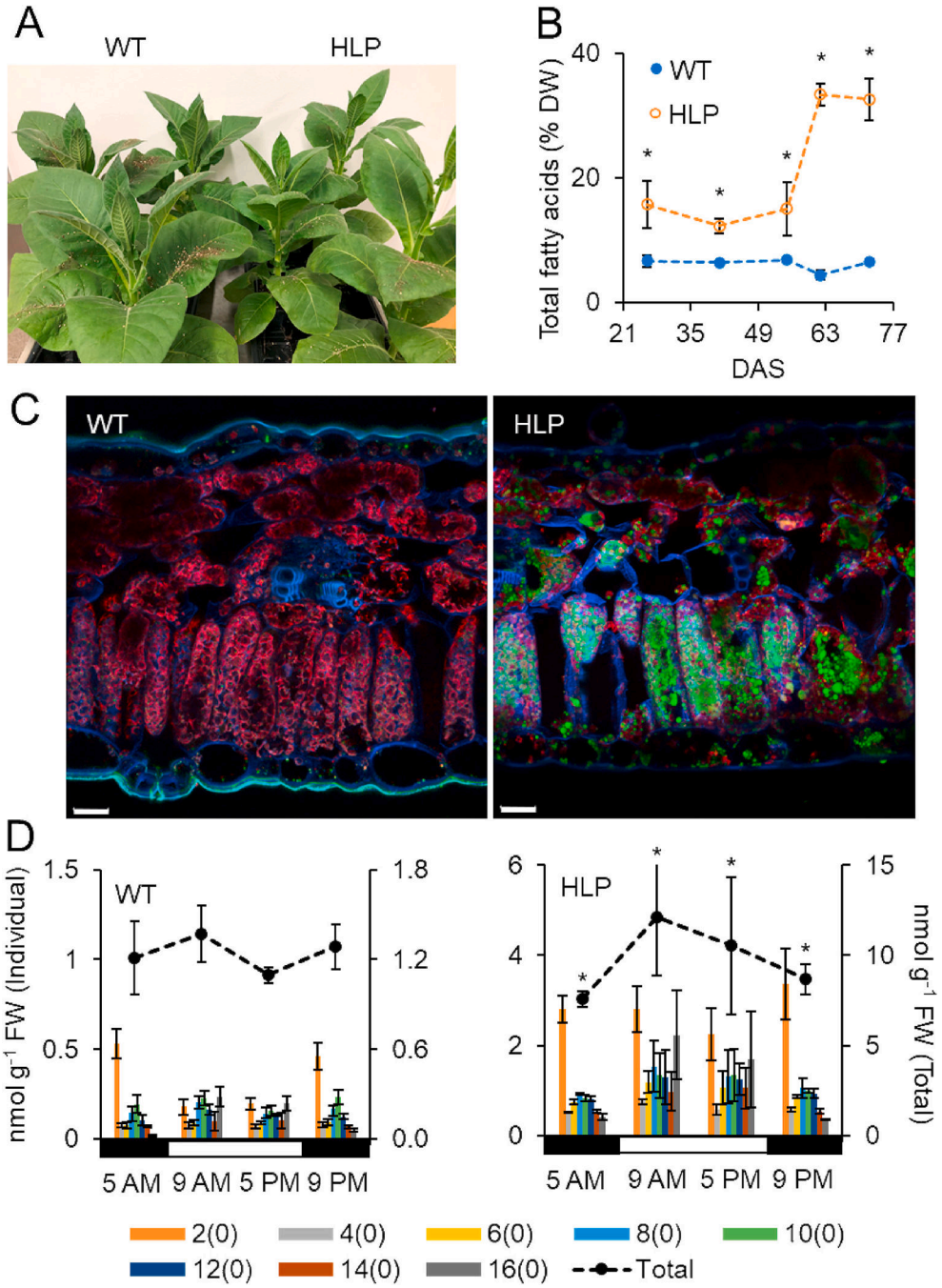

Fig. 1.

Acyl-lipid levels in WT and HLP tobacco leaves over development. (A) WT and HLP plants at 63 days after sowing (DAS). (B) Total fatty acid content of the top expanded leaf of WT and HLP plants sampled at midday across development. The results given are mean ± SD ($n = 3–4$). Asterisks indicate significant differences from WT in the HLP leaves (Student's *t*-test, $P < 0.05$). (C) Accumulation and distribution of lipid droplets in mesophyll cells stained with BODIPY 505/515 (green) in WT and HLP leaf cross-sections. Confocal images are of merged BODIPY 505/515 emission, chlorophyll autofluorescence (magenta), and cell

wall autofluorescence (cyan). Scale bars are 20.01 μm. (D) Diurnal levels of acyl-ACPs from the top expanded leaves of 63 DAS WT and HLP plants assessed over a 12 h L: 12 h D photoperiod. Individual ACPs are presented as bars from two-carbon to a terminal 16-carbon acyl-ACPs. Total acyl-ACP pools are indicated by the line and dot plot above. The results given are mean ± SD ($n = 3$). Asterisks indicate significant differences from WT of total acyl-ACP in HLP leaves (Student's *t*-test, $P < 0.05$).

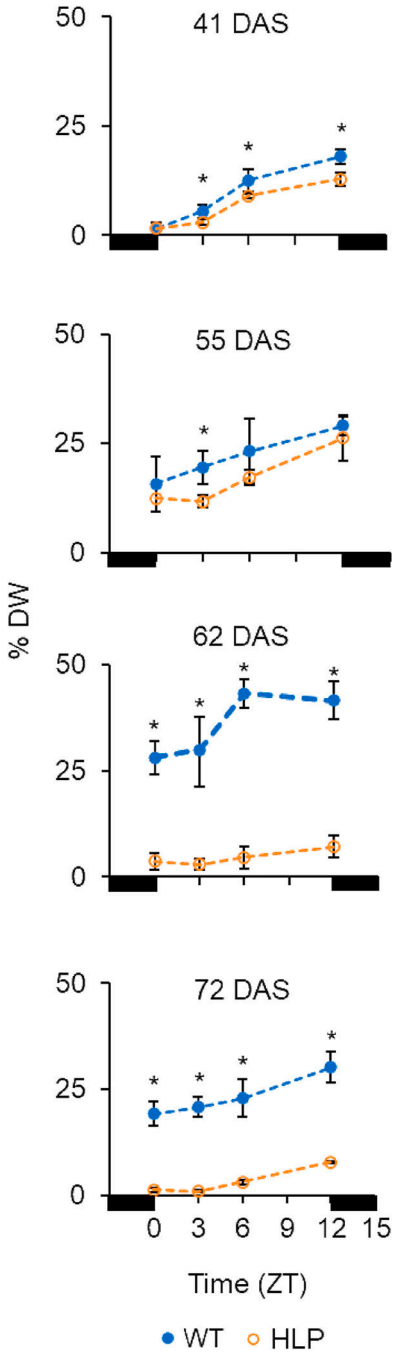

Fig. 2. Diurnal starch levels in WT and HLP leaves over development.

Starch levels in the top expanded leaves of WT and HLP plants over a 12 h L: 12 h D photoperiod at 41, 55, 62, and 72 DAS. Black bars represent darkness. The results given are mean ± SD ($n = 3–4$). Asterisks indicate significant differences from WT (Student's *t*-test, $P < 0.05$).

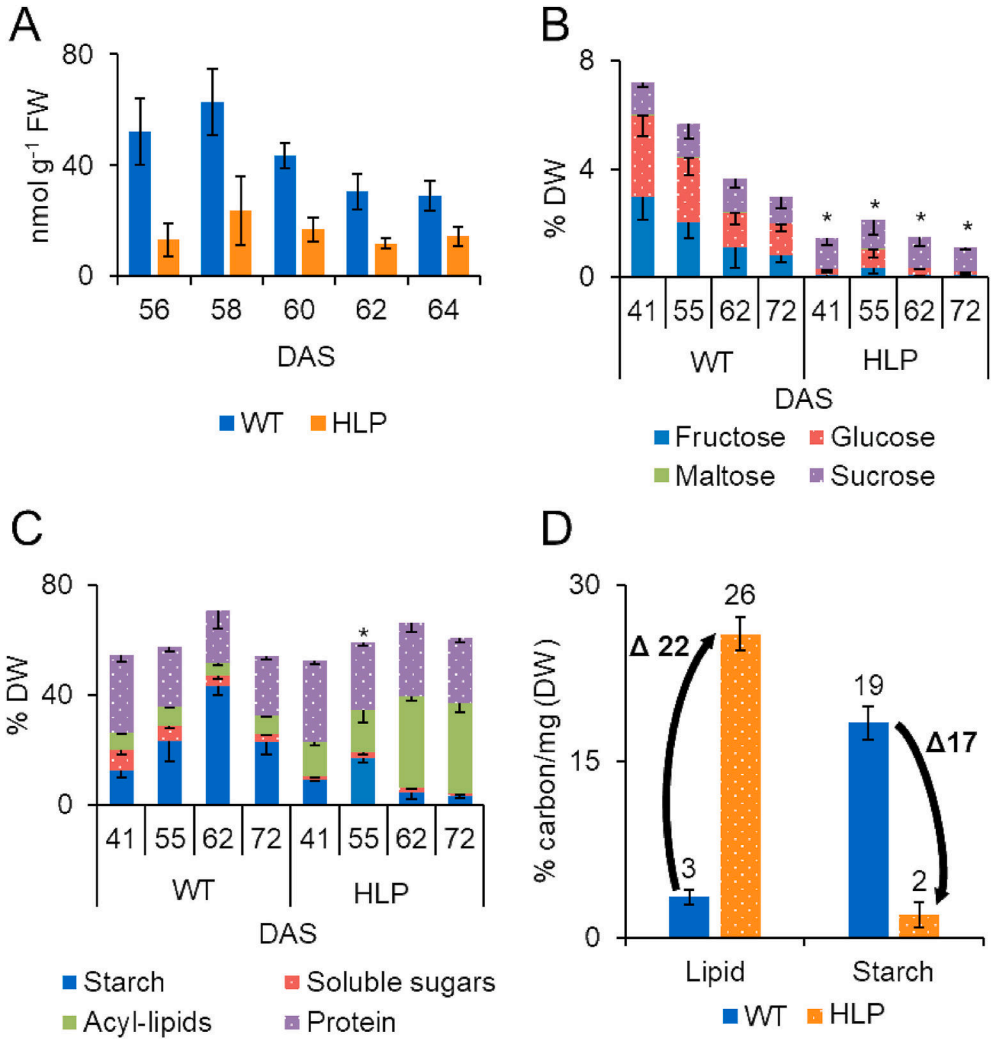

Fig. 3.

Biomass composition changes over development. (A) Maltose levels of WT and HLP leaves between 56 and 64 DAS at midnight. No statistically significant differences were found among HLP levels using ANOVA. (B) Soluble sugar levels in the top expanded leaf of WT and HLP tobacco plants at midday at 41, 55, 62, and 72 DAS. Asterisks indicate significant differences from WT in total soluble sugars in HLP leaves (Student's *t*-test, $P < 0.05$). (C) Total foliar biomass components at midday over development. Asterisks indicate significant differences from WT of protein in HLP leaves (Student's *t*-test, $P < 0.05$). The results given are mean ± SD ($n = 3–4$). (D) Differences in percent carbon per dry weight of WT and HLP lipid and starch values at 62 DAS. Lipid percent carbon was calculated using the proportions and formulas of measured fatty acids, and starch percent carbon was calculated using the formula for maltotriose.

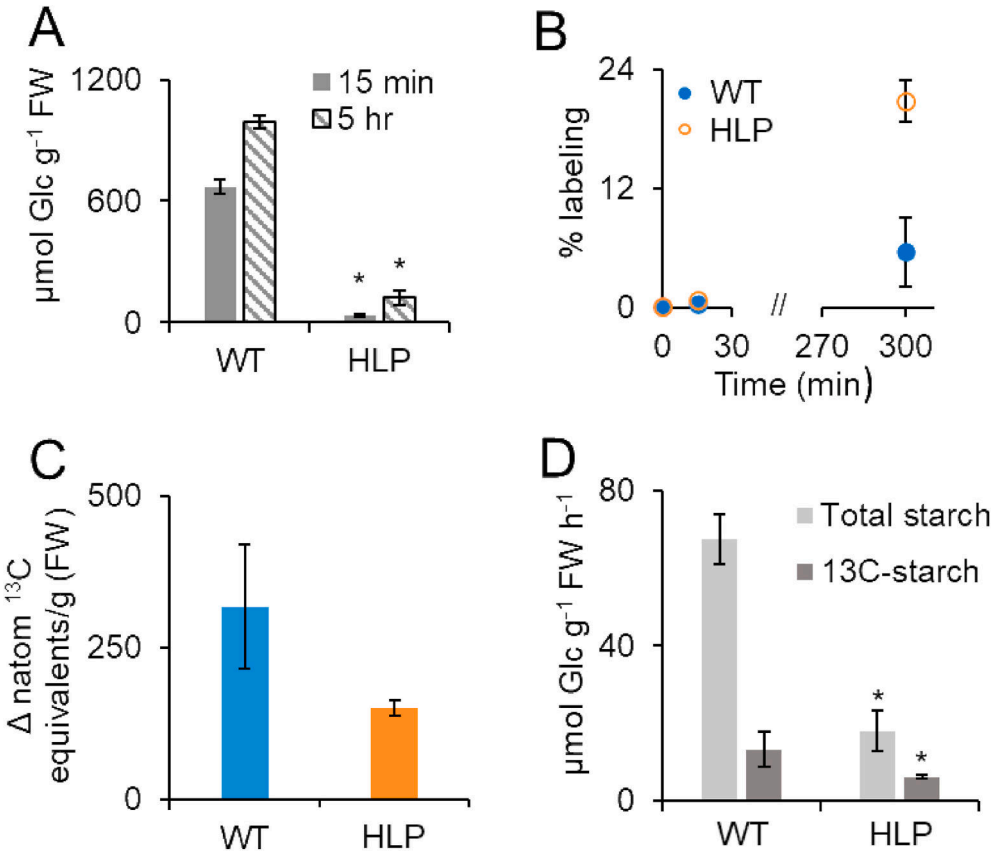

Fig. 4.

Starch production in WT and HLP leaves over the 5 h $^{13}CO_2$-labeling experiment. The top expanded leaves of 62–65 DAS WT and HLP plants were provided with $^{13}CO_2$ and sampled at 15 and 300 min timepoints. (A) Total starch levels at 15 and 300 min. Asterisks indicate significant differences from WT in HLP leaves line (Student's *t*-test, $P < 0.05$). (B) Average % ^{13}C label incorporation (corrected for natural abundance). (C) Amount of ^{13}C in starch produced over the labeling period. ^{13}C amounts (n atom ^{13}C equivalents g^{-1} FW) were calculated as previously described (Arrivault et al., 2016). (D) Differences in total starch production rates (light gray bars) and ^{13}C-labeled starch production rates (dark gray bars). ^{13}C-labeled starch amounts were calculated by summing the labeled isotopologue amounts determined by multiplying isotopologue abundance with the average pool size of starch-digested glucose. The results given are mean ± SD ($n = 3$). Asterisks indicate significant differences from WT in HLP leaves (Student's *t*-test, $P < 0.05$).

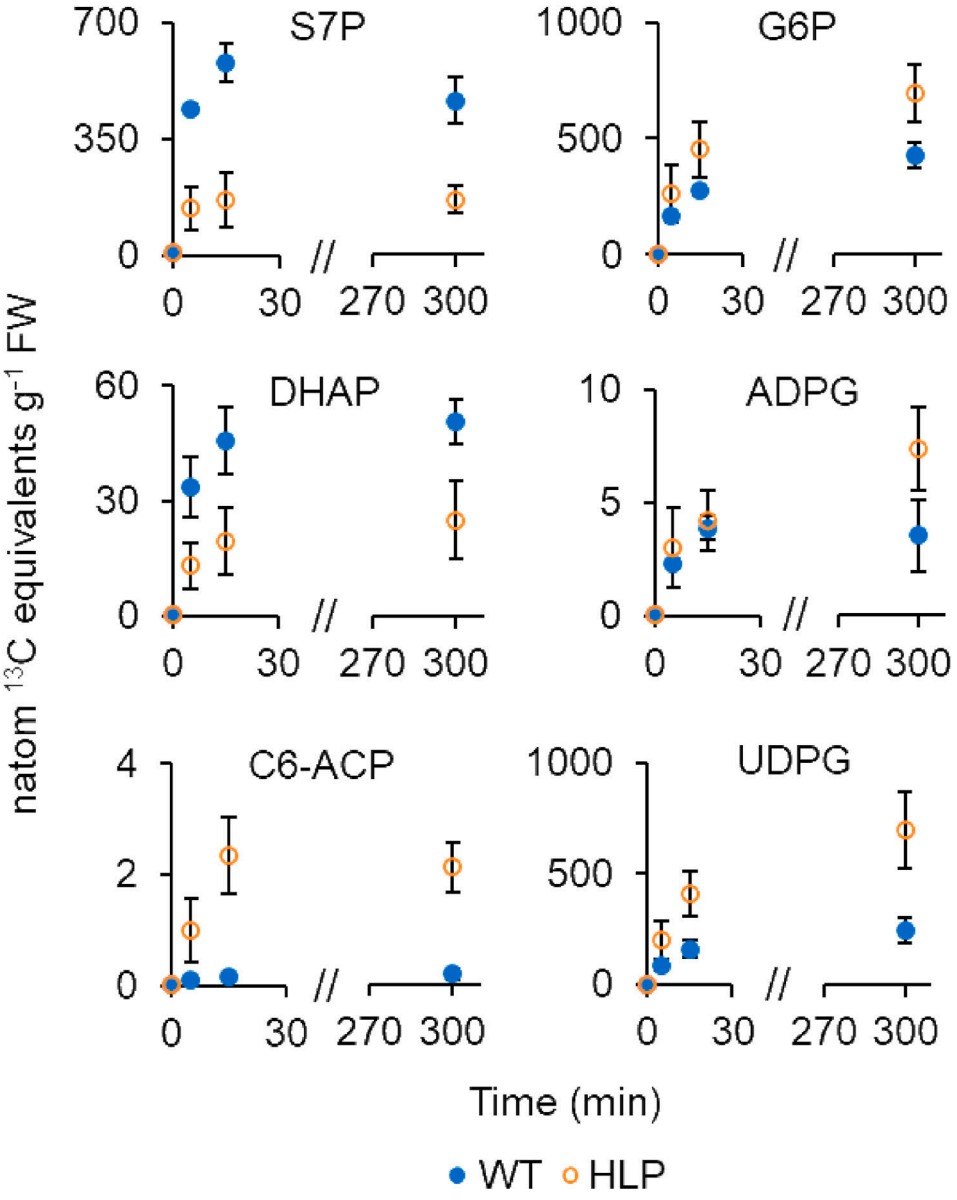

Fig. 5. Visualization of changes in ^{13}C in WT and HLP foliar metabolites.

Labeling kinetics of sedoheptulose 7-phosphate (S7P), dihydroxyacetone phosphate (DHAP), C6-ACP, glucose 6-phosphate (G6P), ADP-glucose (ADPG), and UDP-glucose (UDPG) presented as amount of ^{13}C present in these metabolites over the labeling period. WT labeling patterns are marked in blue and HLP patterns in orange. The results given are mean ± SD (n = 3).

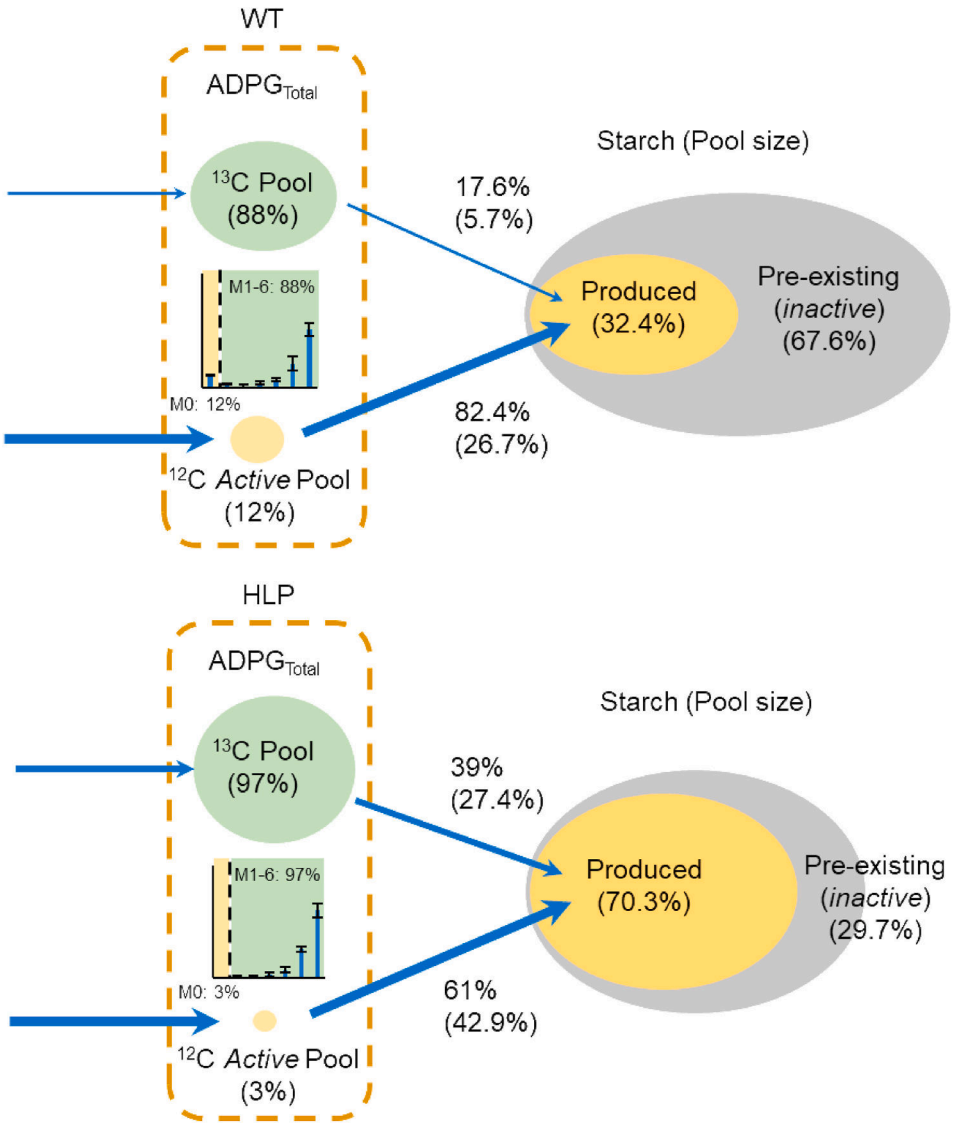

Fig. 6.

Contribution of labeled and unlabeled ADP-glucose to starch production. Relative contributions of 13C-labeled (ΣM1-M6 isotopologues) and unlabeled active (M0 isotopologue) ADP-glucose to starch production over the labeling period in WT and HLP leaves. The contributions are presented as percentages of produced starch and percentages of total starch pool (in parentheses). The data given utilize the means of starch and ADP-glucose isotopologues ($n = 3$), with the proportions of labeled and unlabeled ADP-glucose isotopologues recalculated to be mutually exclusive (Supplemental Datasheet 6).

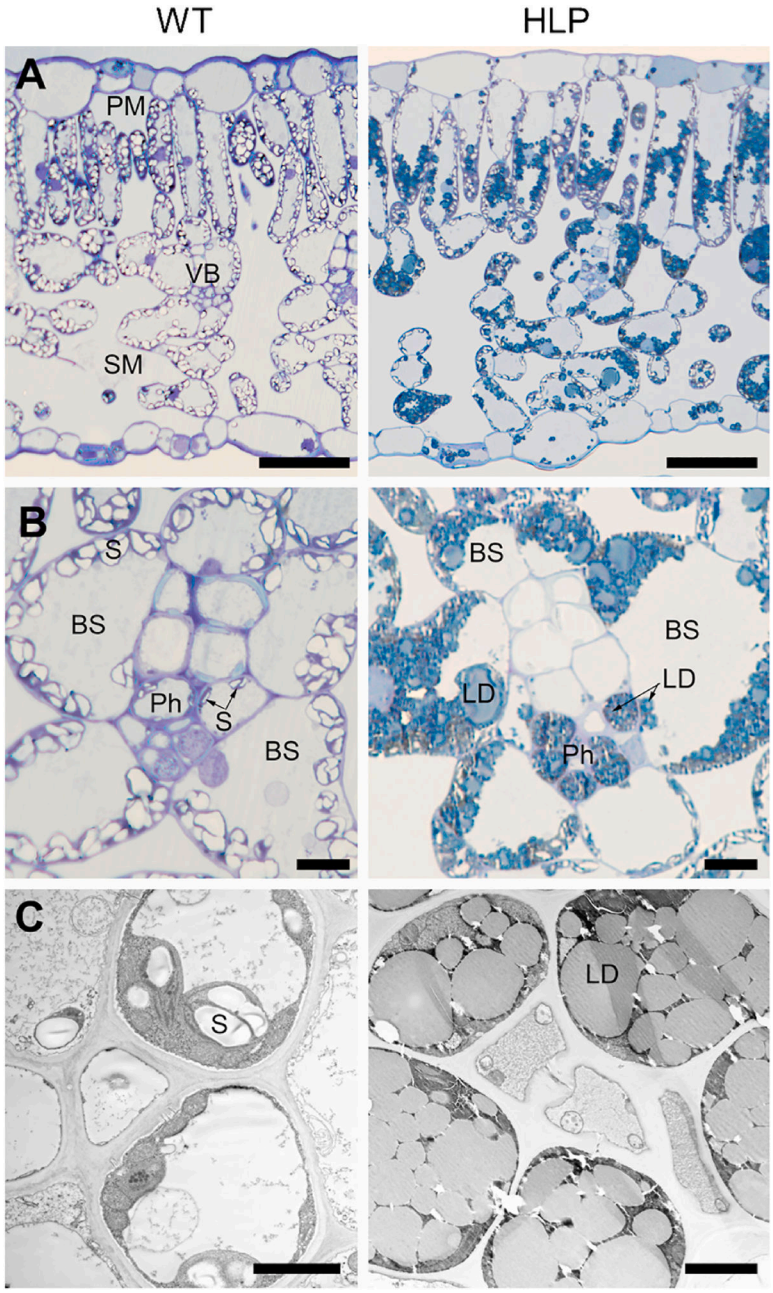

Fig. 7.

Starch and lipid distribution in leaf cross-sections. (A) Light microscopy images of 63 DAS WT (left) and HLP (right) leaf cross-sections at midday stained for lipids (blue). Scale bars are 50 μm. PM, palisade mesophyll; SM, spongy mesophyll; VB, vascular bundle. (B) Light microscopy images of WT and HLP vascular bundles and surrounding bundle-sheath cells at midday. Note the decreased number and size of starch granules in the bundle-sheath cells of HLP leaves and the abundance of lipid droplets (blue). Scale bars are 10 μm. BS, bundle-sheath cell; Ph, phloem cell; S, starch granule; LD, lipid droplet. (C) Transmission electron microscopy images of WT and HLP vascular phloem cells. Note the absence of

starch granules in HLP phloem cells, which are instead packed with lipid droplets. Scale bars are 3 μm.

A

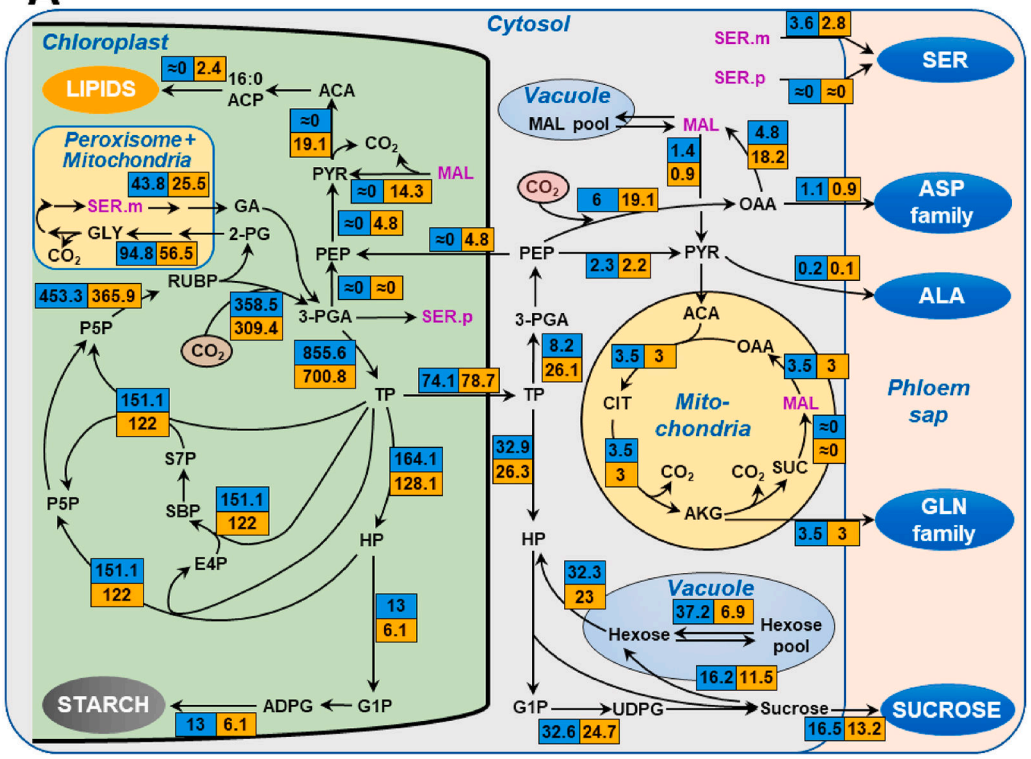

B

Biochemical features	WT	HLP
CO_2 fixation by RuBisCO CO_2 capture by PEPC	98.4% (98.2-98.5) 1.6% (1.6-1.8)	92.4% (94.1-94.4) 5.8 % (5.2-6.4)
Photorespiratory CO_2 produced / total CO_2 produced Lipid biosynthetic CO_2 produced / total CO_2 produced	85.1% (83.7-86.3) < 0.1%	41.2% (37.7-46.1) 48.8% (42.4-55.9)
V_o/V_c	0.26 (0.24 to 0.29)	0.18 (0.16 to 0.22)
Carbon partition into new starch and sucrose synthesis Carbon partition into new starch production Carbon partition into new lipid production	89.3% (78.4-100) 25.3% (20.4-31.6) < 0.1%	44.5% (41.3-47.8) 14.1% (12.1-16.3) 14.7% (12.6-16.9%)
Pyruvate kinase activity in plastidic pyruvate production Malic enzyme activity in plastidic pyruvate production	Flux values < 0.1 Flux values < 0.1	24.9% (12.1-38.4) 75.1% (66.2-85.3)
Cytosolic ME flux / total ME flux Plastidic ME flux / total ME flux	99.5% (94.4-100) 0.5% (0.4-1.2)	5.9% (4.2-8.8) 94.1% (83-100)

Fig. 8.

Carbon fluxes from photosynthetic tobacco leaves determined by INCA. (A) Net flux maps determined from WT and HLP leaves. Flux values shown (WT: blue, HLP: orange) are the medians of the 95% flux confidence intervals and are presented in units of $\mu mol*g^{-1}(FW)*h^{-1}$ (for conversion to carbon flux, multiply by number of carbons). Metabolites in purple are visualized multiple times in different locations on the map but belong to the same pool. All abbreviations used are listed in Supplemental Datasheet 1. (B) Comparison of selected parameters derived from the flux maps (calculations in

Supplemental Datasheet 13). The ranges in parenthesis are the lower and upper bounds at the 95% confidence levels.

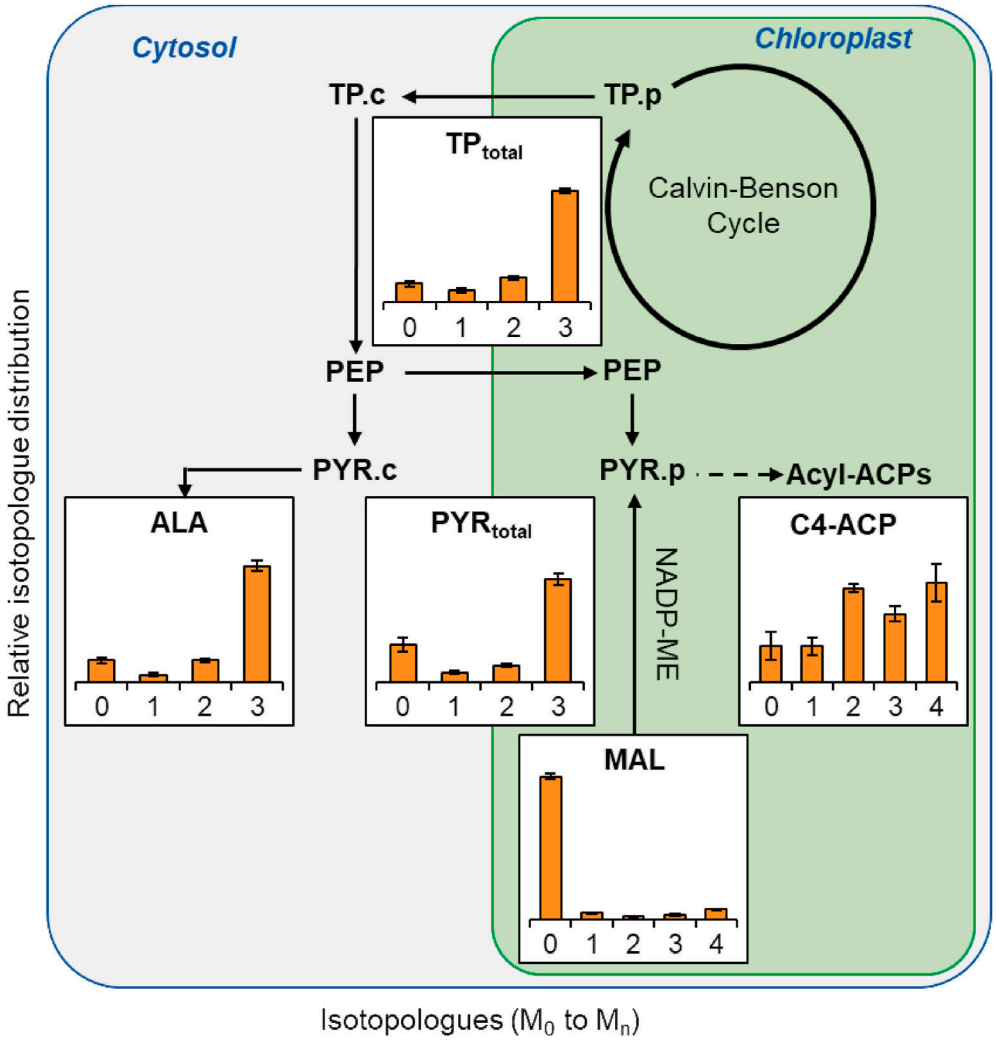

Fig. 9.

Isotopologue distributions of C4-ACP and its precursors after 5 h of labeling in HLP leaves. The high proportion of the M_2 isotopologue of C4-ACP suggests the contribution of unlabeled pyruvate from malate to explain the isotopologue distribution patterns. Note the lower labeling of the total pyruvate pool relative to upstream triose phosphate intermediates and downstream alanine (produced from cytosolic pyruvate). The results given are mean ± SD ($n = 3$).